

# Blockchain-enabled Spectrum Sharing between Satellite and Terrestrial Communication Networks: Architecture, Mechanism, and Analysis

Zixin Wang, Mingrui Cao, Hao Jiang, Bin Cao<sup>\*</sup> *Senior Member, IEEE*, Shuo Wang, Chen Sun<sup>\*</sup>, Xing Liu, and Mugen Peng *Fellow, IEEE*

**Abstract**—Dynamic spectrum sharing (DSS) between satellite and terrestrial networks has increasingly engaged the academic and industrial sectors. Nevertheless, facilitating secure, efficient and scalable sharing continues to pose a pivotal challenge. Emerging as a promising technology to bridge the trust gap among multiple participants, blockchain has been envisioned to enable DSS in a decentralized manner. However, satellites with limited resources may struggle to support the frequent interactions required by blockchain networks. Additionally, given the extensive coverage of satellites, spectrum sharing needs vary by regions, challenging traditional blockchain approaches to accommodate differences. In this work, a partitioned, self-governed, and customized dynamic spectrum sharing approach (PSC-DSS) is proposed for spectrum sharing between satellite access networks and terrestrial access networks. This approach establishes a sharded and tiered architecture which allows various regions to manage spectrum autonomously while jointly maintaining a single blockchain ledger. Moreover, a spectrum-consensus integrated mechanism, which decouples DSS process and couples it with blockchain consensus protocol, is designed to enable regions to conduct DSS transactions in parallel and dynamically innovate spectrum sharing schemes without affecting others. Furthermore, a theoretical framework is derived to justify the stability performance of PSC-DSS. Finally, simulations and experiments are conducted to validate the advantageous performance of PSC-DSS, which achieves up to a 89% reduction in consensus latency and a 375% improvement in throughput compared to baseline approaches.

**Index Terms**—Blockchain, dynamic spectrum sharing, satellite access networks, terrestrial access networks.

## I. INTRODUCTION

SATELLITE access networks (SANs) are envisioned to be broadly supplement to terrestrial access networks (TANs) to realize global seamless coverage, operating in frequency bands below 6 GHz for providing mobile satellite services [1], [2]. The Federal Communications Commission (FCC) has

This work was supported in part by the National Key Research and Development Program of China under Grant 2021YFB1714100, in part by the National Natural Science Foundation of China under Grant No. U22B2006, in part by Research and Development Center, Sony China, and in part by BUPT-China Unicom Joint Innovation Center under grant 2025-STHZ-BJYDDX-008. (\*Corresponding author: Bin Cao, Chen Sun)

Z. Wang, M. Cao, H. Jiang, B. Cao, and M. Peng are with the State Key Laboratory of Networking and Switching Technology, Beijing University of Posts and Telecommunications, Beijing, 100876, China (Email: {Wangzx, caomingrui, jdsxjh, caobin, pmg}@bupt.edu.cn)

S. Wang and C. Sun are with Research & Development Center Sony (China) Ltd., Beijing, 100028, China (Email: {Shuo.Wang, Chen.Sun}@sony.com)

X. Liu is with Research Institute of China United Network Communication Co., Ltd., Beijing 101500, China (Email: liux737@chinaunicom.cn)

recently proposed a regulatory framework to foster spectrum collaboration between TANs and SANs, aiming to offer ubiquitous connectivity [3]. With the increasing of wireless devices and the expansion of satellite constellations, there is a marked escalation in the demand for spectrum resources. However, the spectrum resources at below 6 GHz band have been almost exhaustively licensed while the FCC reports that less than 85% of this band is actually used [4]. High demand and low utilization of spectrum motivate the development of spectrum sharing technologies that reallocate temporarily idle resources between SANs and TANs.

The typical spectrum sharing solutions include static spectrum sharing and dynamic spectrum sharing (DSS). Static spectrum sharing experiences low utilization efficiency due to its fixed and exclusive manner [5]. Thus, DSS is progressively becoming the mainstream to further exploit the potential of limited spectrum resources supply [6]. Several DSS solutions have been developed, such as the well-known spectrum access system (SAS) for citizens broadband radio service (CBRS) [7], and SDN-based designs [8]. However, existing DSS solutions faces major challenges in terms of security and scalability.

For security, all spectrum users must place absolute trust in the spectrum administrators, such as SAS administrators for CBRS [9] and SDN controller [10], who are presumed to be trustworthy to perform reasonable spectrum allocation decisions using a centralized database-based system. This mandatory trust, however, inevitably leads the risk of single point failure and raises security concerns over the malicious exploitation of critical nodes, especially in the evolving threat landscape of SANs. For scalability, centralized DSS models impose excessive regulatory pressure on regulators as an increasing number of heterogeneous participants from regions or countries become involved in SANs, consequently leading to limited scalability. Therefore, a new DSS paradigm that is secure and scalable is in high demand.

As an emerging technology, blockchain has shown the potential to improve the security of DSS due to its ability to enable trust transaction processing and immutable ledger keeping among mutually anonymous participants, even if a certain portion of them behave maliciously [9], [11]. Moreover, the support for the self-executing smart contracts also empowers blockchain to improve the scalability of DSS by distributing responsibility and workload among various participants in a decentralized manner. Many government agencies and organizations have voiced consider blockchain as a possible

paradigm to enable DSS in the future, such as FCC [12], China Communications Standards Association [13], and l'Agence Nationale des Fréquences [14]. Meanwhile, several concrete solutions [15], [16] and innovative studies have been proposed [7], [9], [17]. However, employing blockchain for DSS in SANs still faces the following important challenges:

- *High overhead*: Conventional blockchain-based DSS architecture requires that each transaction be validated by all blockchain nodes. Moreover, additional cross-chain infrastructure is needed to enable interoperability and communication between different chains. This architecture is impractical for DSS in SANs, given the limited resources available on satellites.
- *Limited efficiency*: The prevailing blockchain-based DSS process sequentially allocates distinct portions of the operation to different blocks, with each round of consensus focusing on just one portion. However, this process is time-consuming and power-intensive, which falls significantly short in meeting the crucial needs for both efficient and large-scale spectrum sharing.
- *Constrained flexibility*: Existing blockchain-based DSS solutions require all participants adhere to a unified spectrum sharing scheme, constraining flexibility in the evolving SANs that face a growing diversity of participants with dynamic and varied requirements. For practical purposes, an optimal solution should support for both forward and backward compatibility, especially for SANs undergoing rapid evolution.

Moreover, the characterization of the stability of blockchain systems in SANs is of importance because of ultra-expensive costs for deploying satellites and installing blockchain in satellites. An accurate theoretical framework is essential to thoroughly understand how such systems operate, which kinds of system factors can affect their performance, what the principles that these system factors influence the performance, and further obtain insights on network design guidance [18]. Different from wired networks, the features of SANs, including unstable channel, severe interference, etc., pose many extra difficulties in both theoretical analysis and practical implementations. Therefore, faced with such a complex environment, it is crucial but challenging to consider these features in analyzing the stability of blockchain systems in SANs. However, the study that considers these features simultaneously when applying blockchain to DSS in SANs, is yet inadequate.

The above observations inspire us to develop a partitioned, self-governed and customized DSS approach dubbed PSC-DSS, aiming to provide a low-overhead, highly efficient and flexible DSS solution for SANs. This approach leverages the principle of blockchain to bridge the gap among various parties and establish healthy relationships among diverse spectrum sharing participants in SANs. The main contributions of this work are as follows.

- This work establishes a two-tier multi-region blockchain-based DSS architecture with a single-chain structure, where regions manage spectrum autonomously and synchronize information globally. This architecture allows different regions to adopt various spectrum sharing

schemes and enables interaction across regions without the need for any additional cross-chain infrastructure.

- Based on the proposed architecture, this work designs a spectrum-consensus integrated mechanism, which couples blockchain consensus protocol with spectrum sharing scheme. This mechanism redesigns the consensus protocol and restructures the DSS procedure, enabling regions to parallelly process DSS transactions and dynamically innovate spectrum sharing schemes without affecting others. Furthermore, the generalized workflow and main functions are introduced to advance the understanding of the proposed mechanism.
- A theoretical framework is developed to study the stability performance of PSC-DSS. Based on the derived closed-form expression, we further investigate the impact of the unstable wireless environment in satellite-terrestrial communication on system stability.

Furthermore, simulations and experiments demonstrate the performance of this work in terms of low-overhead, high efficiency, and robust stability under various network parameters. Pivotal insights and design guidelines are provided for further implementations and extensions.

The rest of this work is organized as follows. Section II introduces the overview of PSC-DSS including architecture, entities, and workflow. Section III presents the proposed spectrum-consensus integrated mechanism, detailing the main functions and procedures. Section IV analyses the stability performance. Simulations and experiments are conducted in Section V. Section VI reviews the existing related works. Finally, Section VII concludes this work.

## II. PSC-DSS OVERVIEW

In this section, the architecture of PSC-DSS is first introduced. Then, participants and main tasks are defined. Finally, the work flow of PSC-DSS is described.

### A. Two-tier Multi-region Architecture

As illustrated in Fig.1, the proposed PSC-DSS is composed of two tiers and multiple regions, and all participants maintain only one blockchain.

Tier 1 consists of multiple specific regions, each with a regulator, base stations, and satellites. Each region autonomously manages its spectrum, including the selection and dynamic evolution of suitable spectrum sharing schemes. Transactions related to a specific region are packaged into a block and submitted to tier 2 after the intra-region interaction of the proposed spectrum-consensus integrated mechanism is performed. Accordingly, spectrum sharing can be undertaken separately and parallelly, facilitating efficient and large-scale spectrum sharing in SANs. Furthermore, following this sharding-based design, spectrum management rights are devolved to regions, and promoting more activity and flexible spectral business.

Tier 2, consists of all regulators and many satellites, is responsible for receiving and disseminating the blocks from tier 1, then performing the inter-region interaction of the proposed spectrum-consensus integrated mechanism. After that, all regulators update their world state and blockchain ledger,

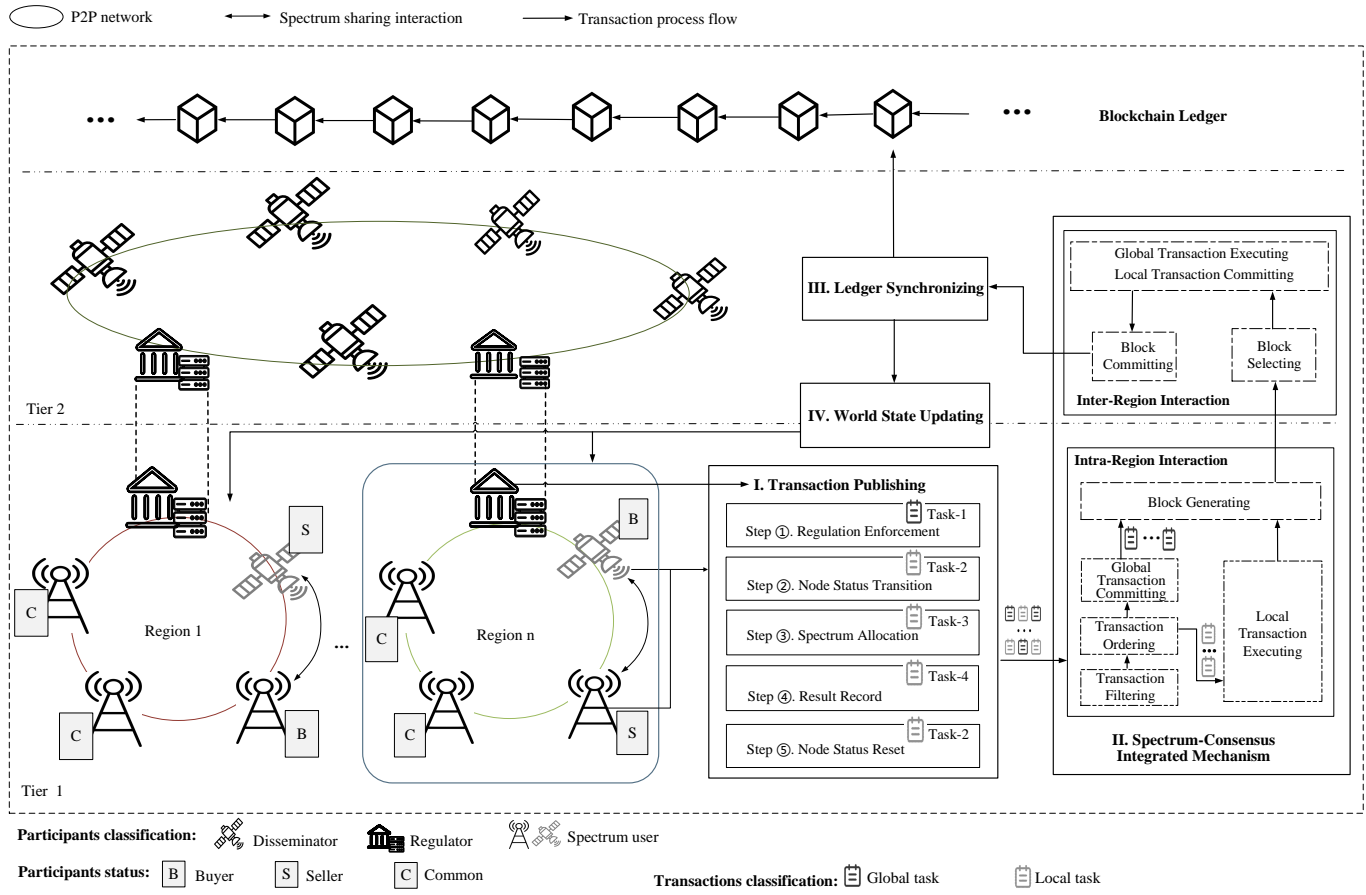


Fig. 1. PSC-DSS architecture

which are then synchronized with base stations and satellites in tier 1. Therefore, all participants record one ledger, reducing resource consumption caused by maintaining multi-region blockchain networks, especially for resource-constrained satellites. This single-chain design enables any DSS transaction in any region can be traced through the blockchain, thus realizing straightforward but trustworthy cross-region supervision and enhancing the recognition of on-chain DSS transactions.

Moreover, PSC-DSS demonstrates robust backward and forward compatibility, allowing for integration with existing distributed spectrum sharing systems. An example of PSC-DSS instantiation is seen in CBRS, where the concept of a “region” aligns with a CBRS “zone” and the “tier” concept corresponds to the relationship between the FCC and CBDS. Furthermore, PSC-DSS supports the dynamic evolution of spectrum sharing schemes for each region by updating a key function in the proposed spectrum-consensus integrated mechanism (detailed in Section IV), without impacting others.

### B. Participants

PSC-DSS involves 3 types of participants: regulators, spectrum users, and disseminators. These participants each play a critical role in spectrum sharing system and blockchain system.

**Regulators** are spectrum management entities that publish regulations on spectrum sharing in their jurisdiction, and provide regulation-compliant spectrum allocation service to

spectrum users. For example, regulators can be distributed FCC entities to make regulations for spectrum sharing, or they can be SAS servers that perform specific schemes. In blockchain networks, regulators initiate a round of intra-region interaction in tier 1, submit the generated region block to satellites in tier 2, and perform the inter-region interaction in tier 2.

**Spectrum users** include base stations and satellites in tier 1 for spectrum access assignment. A spectrum user are categorized into 3 status: buyer, seller, and common. Buyer status indicates that a spectrum user needs additional spectrum to meet specific demands, while seller status represents one with surplus spectrum available for sublease. Common status refers to the spectrum users with stable demand who neither need to buy nor sell spectrum. In blockchain network, spectrum users are responsible for performing intra-region interactions as directed by the regulator in their region.

**Disseminators** are consisted of satellites with no spectrum access needs in their region, considering potential security risks from interest entanglements. They are responsible for receiving blocks submitted by regulators and propagating these blocks in tier 2. A bootstrapper is activated in a selected disseminator to order the blocks and bootstrap regulators for a new round of inter-region interaction.

Disseminators do not participate in spectrum sharing and consensus process. Thus, only regulators and spectrum users

are defined as **blockchain participants**, responsible for transaction verification, task execution<sup>1</sup>, and ledger update.

### C. Main Tasks

In PSC-DSS, spectrum sharing-related tasks are typically classified into 4 types. Task-1 is a global task requiring coordinated implementation in tier 2, while Tasks 2 to 4 are local tasks executable within a specific region. Each type of task can be derived into many blockchain transactions, and a blockchain transaction can contain multiple types of tasks.

**Task-1 Regulation formulation:** PSC-DSS allows regulators to issue rules on various tasks, such as identifying spectrum regions, specifying interference models, and updating participant's information. It is the action guideline for spectrum sharing schemes, and all subsequent spectrum sharing-related tasks are performed on this basis.

**Task-2 User status transition:** Spectrum users specify their spectrum needs, including frequency band, current status and target status, duration of use, and other relevant details. Regulators publish this task to reset the status of spectrum users after completing a round of spectrum allocation process.

**Task-3 Spectrum allocation:** PSC-DSS performs spectrum sharing based on user requests, including parameters for predefined spectrum sharing scheme, user information contained in Task-2, and other required details. Various customize spectrum sharing schemes are allowed to lunched in difference regions to suit their actual situation.

**Task-4 Result record:** Irreversible spectrum requests, allocation results, and current spectrum status are recorded. This task provides a complete track of the spectrum sharing process for all frequency band. Thus, efficient supervisions and audits can be implemented based on this task.

To reduce the overhead of base stations and satellites, PSC-DSS stipulates that only Task-2 is issued by spectrum users during their spectrum application stage, while all other tasks are issued by regulators.

### D. Main Workflow

Since the PSC-DSS is envisioned to be broadly interoperative and to support multiple advanced wireless services and standards, this work focuses on the most basic spectrum sharing approach for which the procedure is shown in Fig. 1.

In step ①, the preparation for spectrum sharing, regulators should issue transactions for Task-1 to publish regulations on spectrum management. This step may be performed periodically or irregularly, depending on updates to spectrum sharing regulations, changes in current spectrum sharing requirements, and evaluations for spectrum sharing implementation plans.

In step ②, spectrum users initiate status requests to regulators to publish transactions for Task-2. For example, if a user has idle spectrum available for sublease, its status in the corresponding frequency band is changed from common to seller. Details about the information and parameters for

<sup>1</sup>If the computational capacity of satellites is insufficient to support transaction execution, the workload can be alleviated by executing tasks on trusted ground proxies or by employing methods such as those described in [19]–[22].

subsequent spectrum allocation in step ④ are submitted to the system.

In step ③, transactions for Task-3 are published by regulators to trigger the specific spectrum sharing schemes. An explicit spectrum allocation solution is obtained for all frequency bands on sale, encompassing spectrum access decisions, operational parameters, business settings, etc.

In step ④, regulators publish transactions for Task-4 to record the whole spectrum sharing process. For a specific frequency band, transfer details such as involved users and operational parameters are recorded. For a spectrum user, specifics in request, transitions in status, changes in assets are captured.

In step ⑤, user's status is reset as common through the transactions pertain to Task-2 published by regulators. This step marks the end of this round of spectrum sharing. If a user has a persistent requirement to maintain a certain status, it needs to re-initiate Task-2 as a new transaction in step1, considering the rapid changes in terms of network topology, channel usage, and participants in SANs.

Each of the above steps is completed by executing a blockchain transaction, as described below.

In Step I, all transactions for tasks are published by regulators to reduce the operational overhead of base stations and satellites. Although Task-2 is initiated by users to actively change their status, users only send requests to regulators, who generate transactions after accumulating a certain number or after a fixed period.

Step II involves perform the proposed spectrum-consensus integrated mechanism. Transactions are packaged into blocks and executed by blockchain participants. Specifically, transactions for global tasks are executed by regulators, while transactions for local tasks are executed by blockchain participants within corresponding regions. Only the results of these executions are recorded in blocks.

Each blcokchain participant updates its local ledger copy in step III. This process ensures that all blcokchain participants possess the same and up-to-date block in ledger. It achieves consistency and completeness in the spectrum sharing process across the network, guaranteeing that all transactions and blocks are correctly recorded and confirmed.

Accordingly, in step IV, the world state is first updated in regulators and then propagated to base stations and satellites. Details pertaining to all tasks are recorded and updated to ensure the accuracy and currency of spectrum management in the PSC-DSS.

## III. SPECTRUM-CONSENSUS INTEGRATED MECHANISM

In this section, the main components for the proposed spectrum-consensus integrated mechanism are first introduced. Then, key functions and procedures are detailed.

### A. Main Components

The proposed mechanism shown in Fig. 2, comprises intra-region and inter-region interactions, which couples spectrum sharing scheme with blockchain consensus protocol.

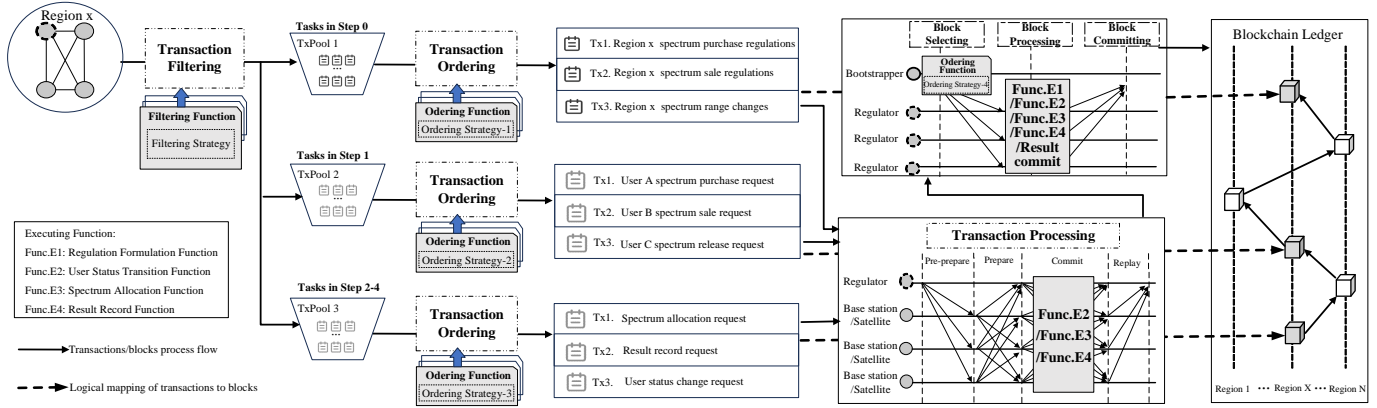


Fig. 2. The process of spectrum-consensus integrated mechanism

### 1) Intra-region Interaction:

The intra-region interaction consists of 3 steps: transaction filtering, transaction ordering, and transaction processing. Through these steps, transactions for local tasks are executed and packaged into blocks.

*Transaction filtering:* As the execution modes and participants of tasks vary across the steps ①-⑤, regulators employ *Filtering Function* to filter transactions corresponding to tasks into 3 distinct transaction pools (TxPools). TxPool1 stores transactions for Task-1 in step ①, TxPool2 manages transactions for Task-2 in step ②, and TxPool 3 is responsible for transactions related to Tasks 2 to 4 across steps ③ to ⑤. This filtering facilitates asynchronous transaction processing and parallel resource allocation.

*Transaction Ordering:* According to Section III-D, the sequence of executing spectrum sharing tasks critically influences the sharing process. Additionally, the priority of task execution varies and develops across different regions. Thus, regulators utilize *Ordering Function* to determine the sequence of transactions taken from TxPool in a block. Due to the transactions in TxPool3 are processed sequentially, they should be ordered following a fixed rule and be packaged into one block. Other transactions can correspond to a different ordering strategies, allowing for adaptive and logical management at each step of the spectrum sharing process.

*Transaction Processing:* Each blockchain participant invokes *Executing Function* to execute transactions. These functions are specifically identified as Func.E2, Func.E3, and Func.E4, detailed in Section III-B. To be specific, a regulator packages the ordered transactions into a block and broadcasts it to blockchain participants within its region. For the block containing transactions from TxPool1, the practical byzantine fault tolerance (PBFT) consensus protocol is initiated. For the block with transactions from TxPools2 or TxPools3, during the *commit* stage of PBFT consensus protocol, blockchain participants trigger the corresponding executing functions (e.g., Func.E2 for TxPool2, Func.E3, Func.E4, Func.E2 sequentially for TxPool3). Then, the processed results replace the original transactions in the block to form a new block. Subsequently, commit message for this new block is generated and broadcast

to all blockchain participants. Once the regulator receives commit messages from more than  $\frac{2}{3}$  blockchain participants in its region [23], [24], it confirms the validity of the new block. Upon validation, the block is then broadcast to disseminators, marking the completion of intra-region interactions and triggering the start of the next round.

### 2) Inter-region Interaction:

After receiving blocks from regulators, disseminators transmit these blocks to all disseminators and regulators through inter-satellite links (ISL). Then, the following steps are performed sequentially.

*Block Selecting:* The bootstrapper activated in a selected disseminator triggers the *Ordering Function* to propose a candidate block, and transmit it to all regulators.

*Block Processing:* If the candidate block contains transactions from TxPool1, regulators invoke *Executing Function* (i.e., Func. E1-Func. E4). Then, the execution results replace the regional transactions in the candidate block. Conversely, if the candidate block contains execution results from transactions in TxPool2 or TxPools3, regulators verify these results.

*Block Committing:* After receiving feedback from a majority (more than  $\frac{1}{2}$ ) of regulators [25], the bootstrapper sends a confirmation message to indicate that the candidate block has been authenticated by the whole network. Then, the blockchain ledger and the world state are updated, marking the completion of inter-region interactions and triggering the start of the next round.

## B. Key Functions

As shown in Fig. 2, the proposed mechanism involves 3 types of key functions, which enable specialized transaction execution. Importantly, these functions can vary across different regions and can be dynamically updated. In this work, procedures corresponding to these key functions are presented as use cases to advance the understanding of PSC-DSS.

### 1) Filtering Function:

This function filters transactions to corresponding TxPools according to their types. Based on Section III-C, Global tasks for global operations are placed into TxPool1. *StatusTrans* tasks for user status transitions are allocated to TxPool2.

---

**Algorithm 1** Ordering Function

**Input:** TxPool1, TxPool2, TxPool3, BlPool  
**Output:** Transaction Lists  $TxLists$ , candidate block  $CandiBl$

- 1: **if**  $TxPool1$  is not empty **then**
- 2:     Order  $Tx$  following FCFS model
- 3:     Append them into  $TxLists(1)$
- 4: **end if**
- 5: **if**  $TxPool2$  is not empty **then**
- 6:     Order  $Tx$  following FCFS model
- 7:     Append them into  $TxLists(2)$
- 8: **end if**
- 9: **if**  $TxPool3$  is not empty **then**
- 10:    Order  $SpecAllo\_Intra$  type  $Tx$  into  $AlloTxlist$ ;
- 11:    **for** each  $Tx$  in  $AlloTxlist$  **do**
- 12:       Order the corresponding  $ResRecord$  and  $StatusRest$  type sequentially after the  $Tx$
- 13:       Append  $AlloTxlist$  into  $TxLists(3)$
- 14:    **end for**
- 15: **end if**
- 16: **if**  $BlPool$  is not empty **then**
- 17:     Order blocks following FCFS model
- 18:     Append them into  $CandiBlList$
- 19: **end if**
- 20: **Return**  $TxLists, CandiBl \leftarrow CandiBlList(1)$

---

$SpecAllo$ ,  $ResRecord$ , and  $StatusReset$  tasks, which are for spectrum allocation, result recording, and status resetting respectively, are assigned to TxPool3.

### 2) Ordering Function:

This function sequences transactions taken from TxPools, and decides how the bootstrapper selects the next candidate block from multiple blocks transmitted by regulators. As presented in Alg. 1, this work adopts first-come-first-serve (FCFS) model to order transactions in TxPool1 and TxPool2, appending them to  $TxLists(1)$  and  $TxLists(2)$ . Similarly, a candidate block  $CandiBl$  is selected from the bootstrapper's block pool  $BlPool$ . Especially, for transactions in TxPool3, transactions with  $SpecAllo$  type are first ordered following the FCFS model. Then, for each  $SpecAllo$  transaction, the corresponding  $ResRecord$  and  $StatusReset$  transactions follow sequentially and are appended into  $TxLists(3)$ . Finally, a transaction list  $TxLists$  including ordered transactions for TxPools is generated. Each element of  $TxLists$  (e.g.  $TxLists(1)$ ) will be packaged into one block to be processed.

### 3) Executing Function:

There are 4 functions for transaction execution. Func. E1-Func. E4 are used to execute the Tasks 1 to 4, respectively. Here, a smart contract which includes 4 sub-function (i.e.,  $GloFunc$ ,  $StaFunc$ ,  $AlloFunc$ ,  $RecFunc$ ) is used to perform the information change for Tasks 1 to 4.

In Func.E1, the sub-function  $SC.GloFunc$  in smart contract is triggered to process transactions  $Tx$  with  $Global$  type in  $CandiBl$ . Then the process results will be added to  $CandiBl$  to replace the original transactions to form a new processed candidate block.

In Func.E2 (shown in Alg.2), transactions in  $TxList(2)$  are processed by the sub-function in the smart contract

---

**Algorithm 2** Func.E2 for processing Task-2

**Input:**  $TxLists$ ,  $RecResultTx$ ,  $AlloResultTx$   
**Output:** Region block  $RegBl$ , shareable spectrum list  $SharedSpecList$ , terminal list  $AwaitUserList$

- 1: **if**  $TxLists(2)$  is not empty **then**
- 2:     **for** each  $Tx$  **do**
- 3:       **if**  $Tx$  is for *seller* status **then**
- 4:           Add seller's spectrum to  $SharedSpecList$ ;
- 5:       **else if**  $Tx$  is for *buyer* status **then**
- 6:           Add buyer's terminal to  $AwaitUserList$ ;
- 7:       **end if**
- 8:       Invoke  $SC.StaFunc$ , obtain processed result  $Tx'$
- 9:       Add  $Tx'$  into  $RegBl$
- 10:      **end for**
- 11:     **return**  $RegBl, SharedSpecList, AwaitUserList$
- 12: **end if**
- 13: **if**  $TxLists(3)$  is not empty **then**
- 14:     Collect all  $Tx$  with  $StatusReset$  type
- 15:     invoke  $SC.StaFunc$  to get  $Tx'$
- 16:     Add  $AlloResultTx$ ,  $RecResultTx$ ,  $Tx'$  into  $RegBl$
- 17:     **return**  $RegBl$
- 18: **end if**

---



---

**Algorithm 3** Func.E3 for processing Task-3

**Input:**  $TxLists$ ,  $SharedSpecList$ ,  $AwaitUserList$

**Output:**  $AlloResultTx$ ,  $SpecRecList$

- 1: **if**  $TxLists(3)$  is not empty **then**
- 2:     Add  $Tx$  with  $SpecAllo$  type into  $AlloList$
- 3:     Perform  $SpecSche(AlloList, SharedSpecList, AwaitUserList)$
- 4:     Obtain  $SpecAlloSolution$  and  $SpecRecList$
- 5:     Invoke  $SC.AlloFunc$  to get the result  $AlloResultTx$
- 6: **end if**
- 7: **return**  $AlloResultTx, SpecRecList$

---

( $SC.StaFunc$ ) to change the status of users included in each  $Tx$ . The processed results,  $Tx'$ , are then added to the region block  $RegBl$ . Additional information, including the details of idle spectrum available for sharing and the information about terminals that require spectrum, are recorded by seller nodes in  $SharedSpecList$  and by buyer nodes in  $AwaitUserList$ , respectively. This information is used to facilitate the execution of the spectrum sharing scheme. For transactions in  $TxLists(3)$ , all  $StatusReset$  type transactions are collected and processed by  $SC.StaFunc$  to get a result  $Tx'$ . Then, the transaction  $AlloResultTx$  returned by Func.E3,  $RecResultTx$  returned by Func.E4, and the  $Tx'$  are sequentially added to  $RegBl$ . Here,  $AlloResultTx$  contains the spectrum allocation results, and  $RecResultTx$  details the entire spectrum sharing process.

In Func.E3 (shown in Alg. 3), all  $SpecAllo$  type transactions in  $Txlists(3)$  are first added to the list  $AlloList$ . Then, a spectrum sharing scheme  $SpecSche$  is performed based on  $AlloList$ ,  $SharedSpecList$ , and  $AwaitUserList$ , obtaining an optimal spectrum sharing solution  $SpecAlloSolution$ . According to  $SpecAlloSolution$ ,

the sub-function *SC.AlloFunc* in the smart contract is invoked to update the spectrum information to get the result *AlloResultTx*. Besides, details of the entire spectrum sharing process, including requests, parameters for *SpecSche*, and the current spectrum situation, are recorded in *SpecRecList*.

In Func. E4, all *ResRecord* type transactions in *Txlists*(3) are collected into a list *ResRecordTxList*. Then, *SpecRecList* is appended to *ResRecordTxList* by matching its elements. Then, *SC.RecFunc* is used to process *ResRecordTxList* and get a result *RecResultTx*.

#### IV. PERFORMANCE ANALYSIS

In this section, the stability performance of PSC-DSS is analyzed in the perspective of the consensus success rate  $P_S$ , and the closed form of  $P_S$  is derived.

##### A. Network Model

Consider a satellite-terrestrial communication system with  $M$  regions, each one contains  $N_s$  satellites and  $N_g$  ground nodes (including a regulator's entity and base stations). Satellites and base stations, as critical components of communication infrastructure, are highly prioritized for their security performance by nations and regions. Accordingly, we assume that the communication and blockchain protocols are inherently secure. However, the communication links remain vulnerable due to the shared spectrum usage among multiple nodes, aimed at reducing spectrum costs. Besides, the blockchain participants are assumed to be rational and trusted<sup>2</sup>, due to the adoption of the consortium blockchain concept in PSC-DSS.

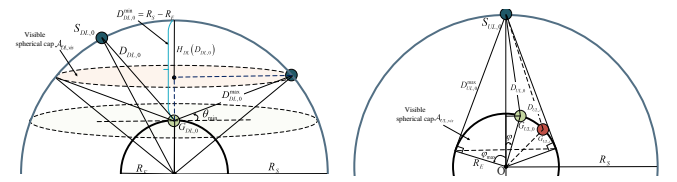
We assume that the satellites are located on the surface of the sphere with radius  $R_S$  according to a homogeneous spherical Poisson point process (SPPP)  $\Phi_S$  with density  $\lambda_s$ . The locations of ground nodes are further assumed to be distributed on the surface of the Earth with radius  $R_E$  according to a homogeneous SPPP  $\Phi_G$  with density  $\lambda_g$ . As shown in Fig. 3, the visible spherical caps of the ground node  $G_{DL,0}$  with minimum elevation angle  $\theta_{\min}$  and the satellite  $S_{UL,0}$  with maximum Earth-centered zenith angle  $\varphi_{\max}$  are denoted as  $\mathcal{A}_{DL,vis}$  and  $\mathcal{A}_{UL,vis}$ , respectively.

For the channel model, the Shadowed-Rician fading model is used for the channels between satellites and ground nodes [26]. Following with [27], a gamma random variable is used to approximate the probability density function (PDF) of channel gain  $|h|^2$ , which is expressed as

$$f_{|h|^2}(x) = \frac{1}{\beta^\alpha \Gamma(\alpha)} x^{\alpha-1} \exp\left(-\frac{x}{\beta}\right), \quad (1)$$

where  $\Gamma(\cdot)$  is the gamma function,  $\alpha = \frac{m(2b_0\Omega)^2}{4mb_0^2 + 4mb_0^2\Omega + \Omega^2}$  and  $\beta = \frac{2b_0 + \Omega}{\alpha}$  is the shape and scale parameters, respectively.  $m$ ,  $2b_0$ , and  $\Omega$  denote the Nakagami fading coefficient, the average power of scattered component, and the average power of line-of sight component, respectively.

<sup>2</sup>Considering potential adverse cases, some blockchain participants may be untrustworthy or malicious for unfair competition. Our system performance analysis model also accommodates the evaluation of such cases.



(a) Downlink satellite-terrestrial net- (b) Uplink satellite-terrestrial works

Fig. 3. Illustration of the geometry of downlink and uplink satellite-terrestrial networks

Hence, the received signal-to-interference-plus-noise ratio (SINR) at  $G_{DL,0}$  for the downlink and at  $S_{UL,0}$  for the uplink can be expressed as

$$\gamma_{DL,0} = \frac{|h_{DL,0}|^2 D_{DL,0}^{-2}}{\bar{\sigma}_G^2 + \sum_{i \in \Phi'_S} |h_{DL,i}|^2 \bar{g}_{DL} D_{DL,i}^{-2}}, \quad (2)$$

and

$$\gamma_{UL,0} = \frac{|h_{UL,0}|^2 D_{UL,0}^{-2}}{\bar{\sigma}_S^2 + \sum_{j \in \Phi'_G} |h_{UL,j}|^2 \bar{g}_{UL} D_{UL,j}^{-2}}, \quad (3)$$

respectively.  $\Phi'_S = \Phi_S \cap \mathcal{A}_{DL,vis} \setminus \mathcal{A}'_{DL,vis}(D_{DL,0})$ ,  $\Phi'_G = \Phi_G \cap \mathcal{A}_{UL,vis} \setminus \mathcal{A}'_{UL,vis}(D_{UL,0})$ ,  $\mathcal{A}'_{DL,vis}(D_{DL,0})$  and  $\mathcal{A}'_{UL,vis}(D_{UL,0})$  denote the visible spherical cap with the maximum distance  $D_{DL,0}$  and  $D_{UL,0}$ , respectively.  $|h_{DL,i}|^2$  and  $|h_{UL,j}|^2$  denote channel gains,  $D_{DL,i}$  is the distance between  $G_{DL,0}$  and the  $i$ th interference satellite,  $D_{UL,j}$  is the distance between  $S_{UL,0}$  and the  $j$ th interference ground node,  $\bar{\sigma}_G^2 = \frac{\sigma_G^2}{P_t^G g_{DL,0}}$  and  $\bar{\sigma}_S^2 = \frac{\sigma_S^2}{P_t^S g_{UL,0}}$  are normalized noise powers.  $P_t^G$  and  $P_t^S$  denote the transmit powers at ground nodes and satellites, respectively. The noise powers at  $S_{UL,0}$  and  $G_{DL,0}$  are  $\sigma_S^2$  and  $\sigma_G^2$ . For the uplink,  $g_{UL,y}$  denotes the effective antenna gain [28] from  $G_{UL,y}$  ( $y \in \{0, j\}$ ) to  $S_{UL,0}$ , with  $g_{UL,0} = g_t^G g_r^S \left(\frac{c}{4\pi f_c}\right)^2$  and  $g_{UL,j} = \bar{g}_{UL} g_{UL,0}$ . Similarly, for the downlink,  $g_{DL,x}$  is the effective antenna gain from  $S_{DL,x}$  ( $x \in \{0, i\}$ ) to  $G_{DL,0}$ , with  $g_{DL,0} = g_t^S g_r^G \left(\frac{c}{4\pi f_c}\right)^2$  and  $g_{DL,i} = \bar{g}_{DL} g_{DL,0}$ . Here,  $g_t^G$  and  $g_r^G$  ( $g_t^S$  and  $g_r^S$ ) are the transmit and receive antenna gains<sup>3</sup> of ground nodes (satellites),  $c$  is the speed of light,  $f_c$  is the carrier frequency, and  $\bar{g}_{UL}, \bar{g}_{DL} \in [0, 1]$  are the uplink and downlink interference mitigation factors [30].

##### B. Success Rate of Reaching Consensus

To quantitatively measure the stability performance of PSC-DSS in SANs, the introduction of a specific performance metric is indispensable. Considering the complex environment of SANs, such as unstable channel and sever interference, satellites and ground nodes are inevitably faced with faulty probabilities, denoted as  $P_f^S$  and  $P_f^G$ , respectively, which significantly affect the consensus reaching process in intra-region interaction and the inter-region interaction.

<sup>3</sup>Directional beamforming with fixed-beam antennas is adopted at the satellites and ground nodes [29].

Hence, the success rate of reaching consensus in both intra-region interaction and the inter-region interaction,  $P_S$ , is defined as the stability performance metric for PSC-DSS in SANs. In PSC-DSS, the intra-region interaction tolerates no more than  $\left\lfloor \frac{N_g+N_s}{3} \right\rfloor$  faulty nodes (including satellites and ground nodes) based on PBFT consensus protocol, and the inter-region interaction requires no more than  $\left\lfloor \frac{M}{2} \right\rfloor$  faulty regulators to commit a block. In such case,  $P_S$  is given as

$$P_S = \sum_{i=0}^{\left\lfloor \frac{N_g+N_s}{3} \right\rfloor} \left[ \left( \sum_{n=0}^{\min(i, N_g-1)} (1 - P_f^G) P_{n0} \right) \left( \sum_{j=0}^{\left\lfloor \frac{M}{2} \right\rfloor} P_j \right) \right] \\ + \sum_{i=1}^{\left\lfloor \frac{N_g+N_s}{3} \right\rfloor} \left[ \left( \sum_{n=1}^{\min(i, N_g)} P_f^G P_{n1} \right) \left( \sum_{j=0}^{\left\lfloor \frac{M}{2} \right\rfloor - 1} P_j \right) \right], \quad (4)$$

with

$$P_{n0} = C_{N_g-1}^n (P_f^G)^n (1 - P_f^G)^{N_g-1-n} \times \mathbf{1}_{\{i-n < N_s\}} \\ \times C_{N_s}^{i-n} (P_f^S)^{i-n} (1 - P_f^S)^{N_s-(i-n)}, \quad (5)$$

and

$$P_j = C_{M-1}^j (P_f^G)^j (1 - P_f^G)^{M-1-j}, \quad (6)$$

where  $P_{n1} = \frac{n(1-P_f^G)}{(N_g-1)P_f^G} P_{n0}$ ,  $\mathbf{1}_{\{\cdot\}}$  is the indicator function, and  $C_a^b$  is the binomial coefficient. See Appendix A for details.

However,  $P_f^G$  and  $P_f^S$  are influenced by various factors, such as security outage and transmission outage probabilities. Considering the inherent security attributes of base stations and satellites, this work mainly measures the faulty probability of nodes from the perspective of transmission outage<sup>4</sup>. For

<sup>4</sup> $P_f^G$  and  $P_f^S$  can also be characterized by considering security outage, e.g.,  $P_f^G = P_{so}^G + P_{out}^G - P_{so}^G P_{out}^G$ , where  $P_{so}^G$  is the security outage probability related to eavesdropping or malicious behavior.

$$\eta(\gamma, \delta, d_{\max}, d_{\min}, g, \kappa, \lambda) = \int_{d_{\min}}^{d_{\max}} \exp(-\beta^{-1}\gamma\delta d^2) \times v(\gamma, d, d_{\max}, \delta, g) \times \zeta(d, d_{\max}, \kappa, \lambda) dd, \quad (9)$$

$$\zeta(d, d_{\max}, \kappa, \lambda) = \frac{2d\pi\lambda\kappa \times \exp(-\pi\lambda\kappa(d^2 + 2R_E R_S - R_E^2 - R_S^2))}{1 - \exp(-\pi\lambda\kappa(d_{\max}^2 + 2R_E R_S - R_E^2 - R_S^2))}, \quad (10)$$

$$v(\gamma, d, d_{\max}, \delta, g) = \sum_{m=0}^{\alpha-1} \left[ \frac{1}{m!} \times \sum_{k=0}^m C_m^k \delta^{2(m-k)} (\beta^{-1}\gamma d^2)^m \times (-1)^k \frac{d^k \chi(\kappa, \lambda, d, d_{\max}, g)}{d(\beta^{-1}\gamma d^2)^k} \right], \quad (11)$$

$$\chi(\kappa, \lambda, d, d_{\max}, g) = \exp \left( \pi\lambda\kappa \left( d_{\max}^2 - d^2 + \frac{(d^2 g \gamma)^{-\alpha}}{\alpha+1} d_{\max}^{2(\alpha+1)} \times {}_2F_1 \left( \alpha, \alpha+1; 2+\alpha; -\frac{d_{\max}^2}{d^2 g \gamma} \right) \right) \right) \\ \times \exp \left( \pi\lambda\kappa \frac{(g\gamma)^{-\alpha}}{\alpha+1} d^2 \times {}_2F_1 \left( \alpha, \alpha+1; 2+\alpha; -(g\gamma)^{-1} \right) \right)^{-1}. \quad (12)$$

$$P_{n,G} = \left[ 1 - \eta \left( \gamma, \bar{\sigma}_G^2, D_{DL,0}^{\min}, D_{DL,0}^{\max}, \bar{g}_{DL}, \frac{R_S}{R_E}, \lambda_s \right) \times \left( 1 - e^{-\pi R_S \lambda_s \frac{(D_{DL,0}^{\max})^2 + 2R_S R_S - R_E^2 - R_S^2}{R_E}} \right) P_{out}^{WL} \right]^n \\ \times \left[ 1 - \left( 1 - \eta \left( \gamma, \bar{\sigma}_G^2, D_{DL,0}^{\min}, D_{DL,0}^{\max}, \bar{g}_{DL}, \frac{R_S}{R_E}, \lambda_s \right) \right) \times \left( 1 - e^{-\pi R_S \lambda_s \frac{(D_{DL,0}^{\max})^2 + 2R_S R_S - R_E^2 - R_S^2}{R_E}} \right) P_{out}^{WL} \right]^{N_g-n}, \quad (14)$$

$$P_{n,S} = C_{N_s}^{i-n} \left[ 1 - \eta \left( \gamma, \bar{\sigma}_S^2, D_{UL,0}^{\min}, D_{UL,0}^{\max}, \bar{g}_{UL}, \frac{R_E}{R_S}, \lambda_g \right) (1 - \exp(-2\pi\lambda_g R_E^2 (1 - \cos \varphi_{\max}))) P_{out}^{ISL} \right]^{i-n} \times \mathbf{1}_{\{i-n < N_s\}} \\ \times \left[ 1 - \left( 1 - \eta \left( \gamma, \bar{\sigma}_S^2, D_{UL,0}^{\min}, D_{UL,0}^{\max}, \bar{g}_{UL}, \frac{R_E}{R_S}, \lambda_g \right) \right) \times (1 - \exp(-2\pi\lambda_g R_E^2 (1 - \cos \varphi_{\max}))) P_{out}^{ISL} \right]^{N_s-(i-n)}, \quad (15)$$

$$P_{j,G} = C_{M-1}^j \left[ 1 - \eta \left( \gamma, \bar{\sigma}_G^2, D_{DL,0}^{\min}, D_{DL,0}^{\max}, \bar{g}_{DL}, \frac{R_S}{R_E}, \lambda_s \right) \times \left( 1 - e^{-\pi R_S \lambda_s \frac{(D_{DL,0}^{\max})^2 + 2R_S R_S - R_E^2 - R_S^2}{R_E}} \right) P_{out}^{WL} \right]^j \\ \times \left[ 1 - \left( 1 - \eta \left( \gamma, \bar{\sigma}_G^2, D_{DL,0}^{\min}, D_{DL,0}^{\max}, \bar{g}_{DL}, \frac{R_S}{R_E}, \lambda_s \right) \right) \times \left( 1 - e^{-\pi R_S \lambda_s \frac{(D_{DL,0}^{\max})^2 + 2R_S R_S - R_E^2 - R_S^2}{R_E}} \right) P_{out}^{WL} \right]^{M-1-j}. \quad (16)$$

a satellite, a fault occurs when it cannot receive signals from other satellites and ground nodes through ISLs and satellite-terrestrial communication links. For ground nodes, a fault occurs when they fail to receive signals through wired and satellite-terrestrial communication links. Therefore,  $P_f^G$  and  $P_f^S$  can be expressed as  $P_f^G = P_{out}^{DL} \times P_{out}^{WL}$  and  $P_f^S = P_{out}^{UL} \times P_{out}^{ISL}$ , respectively. Here,  $P_{out}^{DL}$  and  $P_{out}^{WL}$  are the transmission outage probabilities at ground nodes through the downlink satellite-terrestrial and wired communication links, while  $P_{out}^{UL}$  and  $P_{out}^{ISL}$  are the outage probabilities at satellites via the uplink satellite-terrestrial link and ISLs. Next,  $P_{out}^{DL}$  and  $P_{out}^{UL}$  are derived.

The outage probability is characterized when there is at least one transmitter in visible spherical cap, i.e.,  $\Phi_S(\mathcal{A}_{DL,vis}) > 0$  and  $\Phi_G(\mathcal{A}_{UL,vis}) > 0$ . Thus,  $P_{out}^{DL}$  and  $P_{out}^{UL}$ , are expressed as

$$\begin{aligned} P_{out}^{DL}(\gamma) &= \Pr(\gamma_{DL,0} < \gamma | \Phi_S(\mathcal{A}_{DL,vis}) > 0) \\ &\quad \times \Pr(\Phi_S(\mathcal{A}_{DL,vis}) > 0) \\ &= 1 - \left( 1 - e^{-\pi R_S \lambda_s \left( \frac{(D_{DL,0}^{\max})^2 + 2R_E R_S - R_E^2 - R_S^2}{R_E} \right)} \right) \\ &\quad \times \eta \left( \gamma, \bar{\sigma}_G^2, D_{DL,0}^{\min}, D_{DL,0}^{\max}, \bar{g}_{DL}, \frac{R_S}{R_E}, \lambda_s \right), \end{aligned} \quad (7)$$

and

$$\begin{aligned} P_{out}^{UL}(\gamma) &= \Pr(\gamma_{UL,0} < \gamma | \Phi_G(\mathcal{A}_{UL,vis}) > 0) \\ &\quad \times \Pr(\Phi_G(\mathcal{A}_{UL,vis}) > 0), \\ &= 1 - (1 - \exp(-2\pi\lambda_g R_E^2 (1 - \cos\varphi_{\max}))) \\ &\quad \times \eta \left( \gamma, \bar{\sigma}_S^2, D_{UL,0}^{\min}, D_{UL,0}^{\max}, \bar{g}_{UL}, \frac{R_E}{R_S}, \lambda_g \right), \end{aligned} \quad (8)$$

respectively, where  $D_{DL,0}^{\min} = D_{UL,0}^{\min} = R_S - R_E$ ,  $D_{DL,0}^{\max} = \sqrt{(R_E \sin \theta_{\min})^2 + R_S^2 - R_E^2} - R_E \sin \theta_{\min}$ , and  $D_{UL,0}^{\max} = \sqrt{R_E^2 + R_S^2 - 2R_S R_E \cos \varphi_{\max}}$ .  $\eta(\gamma, \delta, d_{\max}, d_{\min}, g, \kappa, \lambda)$  and the corresponding sub-functions are given in (9)-(12). Details can be found in [31] due to page limitations.

Thus, the closed-form expression for  $P_S$ , reflecting the impact of the complex SANs environment on the stability of the PSC-DSS system, can be derived as

$$P_S = \sum_{i=0}^{\frac{N_s+N_g}{3}} \left[ \sum_{n=0}^{\min(i, N_g)} C_{N_g-1}^n P_{n,G} P_{n,S} \sum_{j=0}^{\lfloor \frac{M}{2} \rfloor} P_{j,G} \right] \\ + \sum_{i=1}^{\frac{N_s+N_g}{3}} \left[ \sum_{n=0}^{\min(i, N_g-1)} C_{N_g-1}^{n-1} P_{n,G} P_{n,S} \sum_{j=0}^{\lfloor \frac{M}{2} \rfloor - 1} P_{j,G} \right], \quad (13)$$

where  $P_{n,G}$ ,  $P_{n,S}$ , and  $P_{j,G}$  are given in (14)-(16).

### C. Communication Complexity

As shown in Fig.1, the communication complexity of PSC-DSS is analyzed in terms of the number of messages exchanged in the intra-region interaction and the inter-region interaction. For the intra-region interaction, there are  $2(N_s + N_g)^2 - 2(N_s + N_g)$  messages sent in the tier 1 network to

package the transaction into a block, due to the adoption of the PBFT consensus protocol. For the inter-region interaction,  $k$  disseminators relay messages between the bootstrapper-activated disseminator and the regulators in regions it does not belong to. Thus,  $4K(M-1)+4$  messages are sent in the tier 2 network. Based on this, for a PSC-DSS with  $K$  disseminators responsible for relaying messages between the disseminator that has the activated bootstrapper and the regulators in regions to which this disseminator does not belong, the communication complexity is

$$\begin{aligned} C &= (N_s + N_g - 1) + (N_s + N_g - 1)^2 \\ &\quad + (N_s + N_g)(N_s + N_g - 1) + 4K(M-1) + 4 + 1 \\ &= 2(N_s + N_g)^2 - 2(N_s + N_g) + 4K(M-1) + 5. \end{aligned} \quad (17)$$

For analytical convenience, assume the number of consensus nodes in each region is equal, the total number of the nodes in the PSC-DSS is  $N = M \times (N_s + N_g) + 1 + \delta K$ , where  $\delta K$  is the total number of disseminators, and  $\delta > 1$  is scale factor. Thus, the optimal communication complexity of PSC-DSS can be given as

$$C_{opt} = O(N^{\frac{2}{3}}). \quad (18)$$

See Appendix B for details.

TABLE I  
SIMULATION PARAMETERS

Parameter	Value
Carrier frequency $f_c$	2 GHz
Satellite transmit power $P_t^S$	30 dBW
Ground transmit power $P_t^G$	33 dBm
Satellite transmit antenna gain $g_t^S$	38 dBi
Satellite receive antenna gain $g_r^S$	37.8 dBi
Ground transmit antenna gain $g_t^G$	38.5 dBi
Ground receive antenna gain $g_r^G$	39.7 dBi
Noise power $\sigma_S^2, \sigma_G^2$	-174 dBm/Hz
Interference mitigation factors $\bar{g}_{UL}, \bar{g}_{DL}$	0.1
Minimum elevation angle $\theta_{\min}$	10°
Max zenith angle $\varphi_{\max}$	$\arccos(R_E/R_S)$
Earth radius $R_E$	6371 km
Satellite orbit radius $R_S$	6871 km
Transmission rate	200 Mbps
Processing speed	2.4 GHz
Costs of generating/verifying the consensus messages	4M CPU cycles
Block header size in tier 1, tier 2	39, 321 bytes
Transaction sizes for Tasks 1, 2, 3, 4	700, 390, 200, 650 bytes
Message sizes for pre-prepare, prepare, commit, vote	800, 200, 215, 800 bytes

## V. PERFORMANCE EVALUATION

This section evaluates the performance of the proposed PSC-DSS in terms of overhead, efficiency, and stability. The evaluation criteria are defined as follows: overhead is assessed through consensus latency, efficiency is measured by transactions per second, and stability by the success rate of reaching consensus.

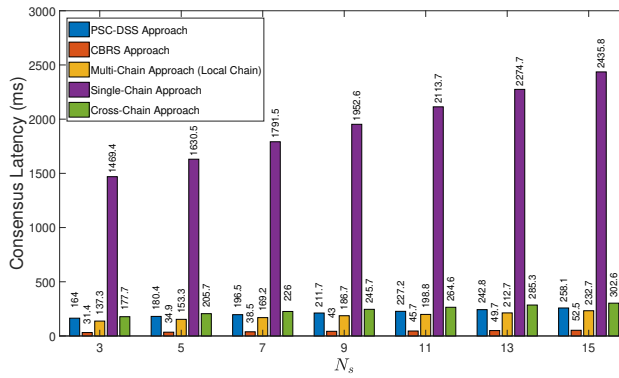


Fig. 4. Consensus latency versus  $N_s$

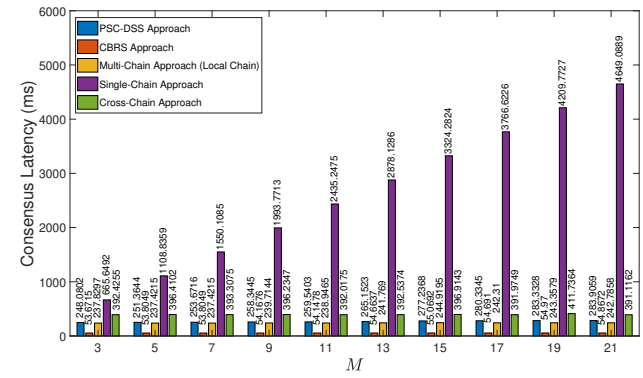


Fig. 5. Consensus latency versus  $M$

### A. Setup

In this work, the common parameter settings are listed in Table I on the basis of the existing works [18], [26], [28], [29], [32].

To evaluate the consensus latency and TPS, we collect ground stations of American from the website: <https://satellitemap.space>, and use the two-line element set of Starlink [33] to construct SANs. Here, ground stations act as regulators, with base stations randomly distributed around each ground station. Each region includes 14 base stations. To evaluate the stability of PSC-DSS for further large-scale deployment, the distributions of ground nodes and satellites are realized by the generation of SPPP and Monte-Carlo simulation is used.

To evaluate the computing consumption and memory consumption, P3-Chain [34] with the advantages of partitioning on transaction, parallelizing on block, and programming on consensus, is applied as the blockchain platform for this work. We run the PSC-DSS on a cloud virtual machine equipped with 128 cores and 256GB of RAM, and implement two spectrum sharing schemes<sup>5</sup>: one to maximize spectrum revenue and the other to minimize aggregated interference.

Baselines are as follows: *CBRS* approach [35] performs spectrum using a centralized SAS in each region, *Single-Chain* approaches [4], [36] use blockchain with PBFT consensus protocol to enable spectrum sharing, *Multi-Chain* approach [7] performs spectrum allocation in local chains while records allocation information in global chain, and *Cross-Chain* [37] approach provides a two-phase-confirmation scheme for communication and synchronization between two local chains. To achieve a unified consensus protocol across different approaches, both the *Multi-Chain* and *Cross-Chain* approaches employ PBFT. The number of transactions in a block is the same as the number of nodes (i.e.,  $N_g + N_s$ ) in a region.

### B. Consensus Latency

Fig. 4 shows consensus latency increases with  $N_s$  when the number of regions is set as  $M = 11$ , due to larger  $N_s$  leads to greater consensus complexity, which in turn raises the

<sup>5</sup>[https://github.com/rebear077/DSS\\_RelevantCode](https://github.com/rebear077/DSS_RelevantCode)

time consumed in propagation, transmission and computing. Compared with *CBRS* approach, PSC-DSS requires more time to reach consensus due to necessary communications among blockchain participants. However, the increase in latency is relatively minor, and PSC-DSS not only enables CBRS sharing within the region but also facilitates inter-region information sharing. Similarly, since PSC-DSS requires interactions among all regulatory for global information synchronization, the latency is slightly higher compared to the local sharing in *Multi-Chain* approach that lack global synchronization. Besides, this figure shows a significant gap between PSC-DSS and *Single-Chain* approach, as PSC-DSS reduces extensive communications needs by implementing sharding and tiering, and achieves up to a 89% reduction in consensus latency when  $N_s = 15$ . Moreover, compared to *Cross-Chain* approach, latency in PSC-DSS is slightly reduced because it only requires consensus among cross-region regulators, not within two separate regions.

Fig. 5 shows consensus latency versus  $M$ . The *CBRS* and *Multi-Chain* approaches are almost unaffected by the changes of  $M$ , since they carry out information dissemination within their region. Slight fluctuations (2-3 ms) are due to randomly generated base station locations. A similar situation occurs in *Cross-Chain* approach because it performs consensus protocol only in the relevant two regions and transmits cross-region information via satellites. In *Single-Chain* approach, consensus latency increases rapidly with  $M$  as the number of participating nodes expands. However, while PSC-DSS's consensus latency also increases with  $M$  due to the growing number of nodes in tier 2 consensus protocol, it still demonstrates slow latency growth, showcasing excellent scalability.

### C. Efficiency

Fig. 6(a) shows the transactions per second (TPS) versus  $M$ . For the *Single-Chain* approach, as  $M$  increases, the number of blockchain participants and transactions rises, rapidly increasing consensus latency due to transmission, propagation, and processing across multiple nodes. This makes it difficult to increase TPS even in this experiment omitting

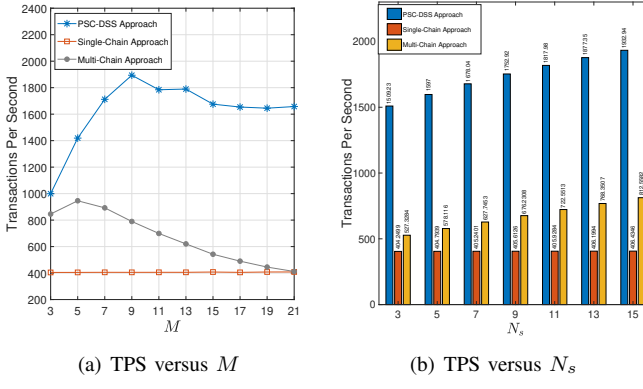


Fig. 6. Transactions per second versus  $M$  and  $N_s$ .

network congestion. For the *Multi-Chain* approach, TPS decreases with  $M$  because allocation record transactions must wait for spectrum allocation transactions to complete intra-region consensus before proceeding to inter-region consensus. Moreover, as  $M$  increases, more nodes participate in the global chain's consensus process, leading to higher consensus latency and consequently reducing TPS. Similarly, the TPS of PSC-DSS slightly decreases with  $M$  due to increased waiting time for candidate blocks submitted by regions to the bootstrapper, and increased consensus latency among all regulators in tier 2. When  $M = 9$ , PSC-DSS achieves up to a 375% improvement in throughput compared to the *Single-Chain* approach. However, PSC-DSS achieves a stable TPS as  $M$  increases. This stability is due to PSC-DSS packaging transactions such as spectrum allocation and recording into one block for consensus, requiring consensus only among regional nodes and regulators across regions. This approach avoids involving all nodes in the consensus and eliminates waiting times associated with sequential block generation for different transactions.

Similarly, Fig. 6(b) shows TPS increases with  $N_s$ . The *Single-Chain* approach is limited in TPS growth because all nodes are involved in global consensus. The *Multi-Chain* approach shows limited TPS due to the need to complete both intra-region and inter-region consensus. In contrast, PSC-DSS significantly improves TPS by adopting a partitioned and hierarchical design that avoids global synchronization and redundant waiting.

#### D. Stability

In this experiment, we first evaluate the correctness of the analysis in (13) under the setting of  $M = 60$ ,  $N_g = 40$ , and  $N_s = 20$ . Fig. 7 shows that the analytical results for  $P_S$  tightly match the simulation results. From Fig. 7(a), we can see that the PSC-DSS can a faulty probability of over 0.7 for satellites when  $P_f^G = 0.03$  and over 0.3 for satellites when  $P_f^G = 0.2$ . Referring to Fig. 7(b), the variation of  $P_f^G$  has a significantly impacts on  $P_S$ , since ground nodes participate in both intra-region and inter-region consensus processes.

Then, we evaluated the success rate of reaching consensus in dynamic and fixed network topologies with varying net-

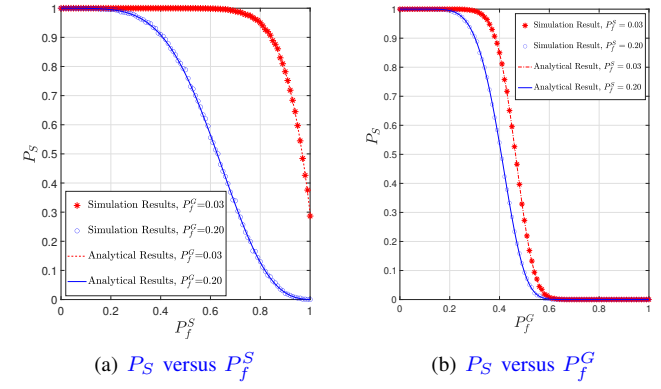


Fig. 7. Success rate of reaching consensus versus faulty probabilities.

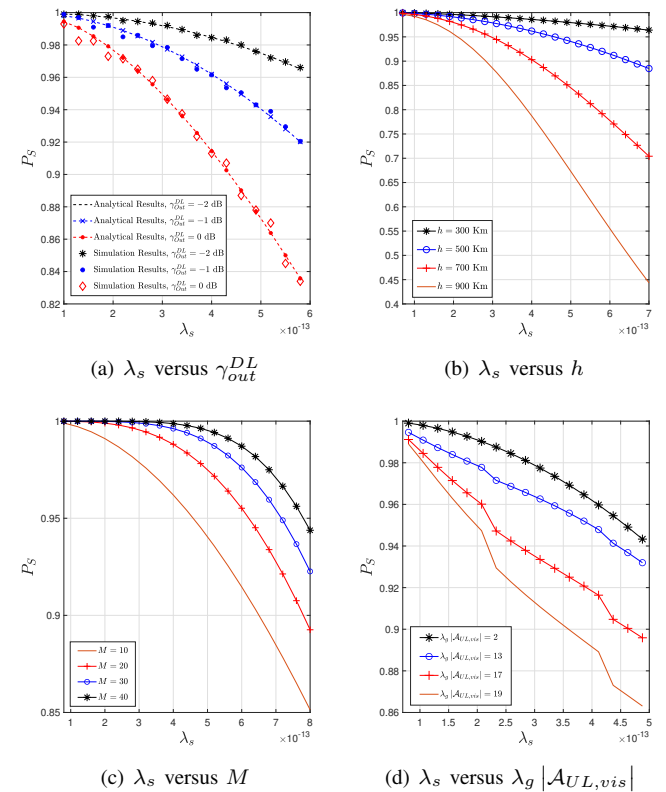


Fig. 8. Success rate of reaching consensus versus satellite density at different network parameters in the dynamic network topology.

work parameters. This revealed how many satellites share a downlink channel and how many ground nodes share a uplink channel for a stable consensus process can be tolerated by the PSC-DSS from the perspective of resource conservation. For dynamic network topology, the number of blockchain participants varies with the density of satellites, where all satellites in  $A_{DL,vis}$  are treated as blockchain participants and share the same downlink channel. For fixed network topology, the number of blockchain participants is fixed, and the density of satellites is related only to the number of satellites share the same downlink channel. Besides, we set  $M = 10$  and  $N_g = 15$ .

**Dynamic Network Topology:** Here, every three ground nodes

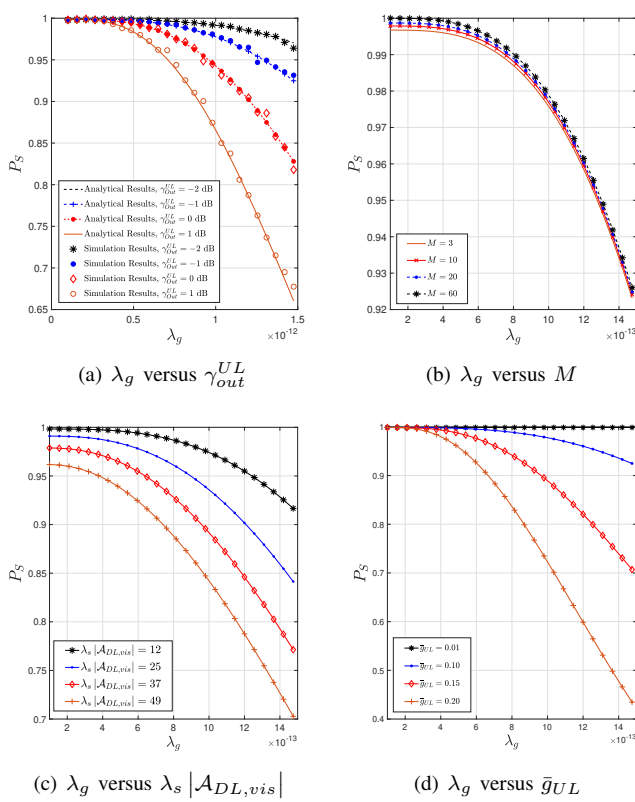


Fig. 9. Success rate of reaching consensus versus satellite density at different network parameters in the fixed network topology.

share an uplink channel with uplink SINR threshold set as  $\gamma_{out}^{UL} = -1$  dB. Fig. 8, we shows  $P_S$  decreases with  $\lambda_s$ . The higher  $\lambda_s$ , the more satellites share the downlink channel, thus leading to a poorer  $P_f^G$ .

Fig. 8(a) first demonstrates the accuracy of the success rate of reaching consensus. The analytical results are computed from (13), and the simulation results are obtained by independent Monte Carlo trials. Although  $P_S$  decreases with the downlink SINR threshold  $\gamma_{out}^{DL}$ , the black curve shows that PSC-DSS can support 72 satellites (i.e.,  $\lambda_s = 6 \times 10^{-13}$  per  $m^2$ ) sharing a downlink channel to reach consensus. For the following experiments, we set  $\gamma_{out}^{DL} = -1$  dB.

Fig. 8(b) shows  $P_S$  decreases with the altitude of satellites,  $h = R_S - R_E$ . As the number of satellites in  $A_{DL,vis}$  increases with  $h$ ,  $P_{out}^{DL}$  for ground nodes rises, leading to a higher  $P_f^S$ . However, this figure shows that PSC-DSS can support over 68, 49, 37, and 27 satellites sharing a downlink channel at altitudes of 300 Km, 500 Km, 700 Km, and 900 Km, respectively.

Fig. 8(c) shows  $P_S$  increases with the number of regions  $M$ . When  $P_{out}^{DL}$  is large but less than 0.5 (such as  $\lambda_s = 6 \times 10^{-13}$  per  $m^2$  for  $P_{out}^{DL} = 0.3416$ ), the system's stability can be enhanced by increasing  $M$ . This is because more regions reduce the probability of more than half of the tier 2 ground nodes failing, thereby improving the success rate of consensus in inter-region interactions.

Fig. 8(d) shows  $P_S$  decreases with the number of ground nodes which share an uplink channel, represented by  $\lambda_g |A_{UL,vis}|$ . A slight change in  $\lambda_g |A_{UL,vis}|$  leads to sig-

nificant changes in  $P_S$  because a greater  $\lambda_g |A_{UL,vis}|$  results in a higher  $P_{out}^{UL}$ . However, as  $\lambda_g$  increases, more satellites experiencing a high  $P_{out}^{UL}$  will participate in the consensus process, causing a rapid decrease in  $P_S$ .

*Fixed Network Topology:* In this experiment, we set  $N_g = 15$  and  $N_s = 20$  and every 10 satellites share a downlink. Similar with above results, Fig. 9 shows  $P_S$  decreases with  $\lambda_g$  due to the growth in number of ground nodes significantly affect  $P_{out}^{UL}$  for satellites.

Fig. 9(a) demonstrates the analytical results exactly matches with the simulation results for all the cases of  $\gamma_{out}^{UL}$ . In such case, the black curve shows the PSC-DSS can support over 27 ground nodes share an uplink channel while maintaining system stability. Fig. 9(b) shows that the increasing  $M$  in this case does not have a significant effect on enhancing system stability  $P_S$  with  $\gamma_{out}^{DL} = -1$  dB. This is because PSC-DSS can maintain a stable consensus process due to the majority of ground nodes in tier 2 are no faulty when  $P_{out}^{DL}$  is small (about 0.1483). Fig. 9(c) shows  $P_S$  decreases as the number of satellites sharing the downlink channel increases, due to the resulting higher downlink outage probability  $P_{out}^{DL}$ , which reduces overall system reliability. Fig. 9(d) further illustrates system stability is highly sensitive to the interference mitigation factors. As interference increases, the probability of transmission failure rises, causing more frequent disruptions in both intra- and inter-region consensus.

#### E. Computing Consumption

Table II shows the average CPU usage rises with  $M$  and the number of nodes in a region (i.e.,  $N_r = N_g + N_s$ ), due to the increased number of transactions to be executed and communication information to be processed. PSC-DSS starts with CPU usage below 7% for up to 64 nodes, which then rises gradually as it scales to 256 nodes and demonstrates a modest upward trend. Furthermore, we can find that bootstrappers are most affected by the increase in the number of nodes, followed by regulators, and finally spectrum users. This is because that spectrum users only process transactions and performs consensus within a region, while regulators need to execute the both, and bootstrappers need to organize network and coordinate the consensus process in tier 2.

#### F. Memory Consumption

Table II also illustrates the average memory usage escalates with the number of nodes. Both regulators and spectrum users exhibit similar patterns in memory consumption. This similarity arises because both types of participants are involved in executing transaction performing consensus process and maintaining a copy of the blockchain ledger. In contrast, the memory usage of the bootstrapper is lower than that of the regulators and spectrum users. The primary reason for this difference is that bootstrappers are not required to execute transaction and maintain a copy of the blockchain ledger. Instead, they only need to store the blocks that have been submitted by each region and boost the consensus process in

TABLE II  
AVERAGE CPU AND MEMORY USAGE BY PARTICIPANTS

Participants	$M \times N_r$							
	$2 \times 4$	$4 \times 4$	$4 \times 8$	$8 \times 4$	$8 \times 8$	$8 \times 16$	$16 \times 8$	$16 \times 16$
<b>CPU Usage (% core)</b>								
Bootstrapper	1.5	3.4	5.5	6.85	6.7	43.85	38.3	53.65
Regulator	2.1	4	5.7	5.2	8.13	17.35	13.5	54.25
Spectrum User	2.5	2.85	4.95	5	5.3	19.8	15.45	49
<b>Memory Usage (MB)</b>								
Bootstrapper	54.3	60.95	56.3	59.9	58.25	67.9	67.35	100.05
Regulator	73.7	77.05	76.4	70.6	80.15	84.85	81.4	100.45
Spectrum User	66.4	71.95	70	76.95	74.9	84.8	79.55	98.75

tier 2. However, as the number of regions increases, so does the number of blocks each bootstrapper needs to manage. This escalation in the number of blocks directly contributes to an increase in memory usage for bootstrappers.

## VI. RELATED WORKS

### A. DSS for SANs

Several efforts have demonstrated the feasibility of DSS in SANs. MediaTek [38]–[40] propose a reverse spectrum sharing mechanism, where instead of SANs' DL channels sharing with each other, the DL shares with an TANs' UL channel. Fair-spectrum [41], [42] designs a spectrum management system to enable dynamic spectrum sharing between SANs and TANs, which utilizes the last historical statistics for dynamic resource sharing. European Space Agency [43] issues a project for licensed assisted spectrum access satellite networks, which considers the implementation of the licensed shared access mechanism to facilitate spectrum sharing between mobile terrestrial networks and satellite system.

### B. Blockchain for DSS

Recently, efforts have highlighted blockchain's potential in DSS, focusing on developing smart contracts, blockchain architectures, and consensus mechanisms.

Using smart contract to perform spectrum sharing schemes is a common approach. Jiang *et al.* [44] propose a smart contract-enabled permissioned blockchain-based dynamic spectrum acquisition scheme. Boateng *et al.* [45] design smart contracts to perform decentralized spectrum trading. Ayepah-Mensah *et al.* [46] employ smart contracts to execute resource allocation and trading process among RANs. Xu *et al.* [47] record the spectrum auction results into a smart contract. Although these efforts enable DSS efficiently, they require all participants to follow a conventional architecture and a unified spectrum sharing scheme. As participant numbers grow, these efforts inevitably face significant bottlenecks due to limited scalability and constrained flexibility in meeting the dynamic and varied needs of participants.

Aiming to improve the scalability of blockchain-based DSS systems, an emerging trend is to establish new architectures incorporating tiered and sharded features. Hu *et al.* [48] introduce a two-tier hierarchical blockchain architecture for DSS, consisting of a global chain in tier 1 and multiple local

chains in tier 2. Local chains are updated to the global chain at a fixed or a dynamic frequency. Xiao *et al.* [9], [17] propose a blockchain-based decentralized SAS architecture, with a global chain used for spectrum regulatory tasks and several local chains for automating spectrum access assignment. Also, the state of local chains is updated on global chain at a fixed frequency. However, these approaches cannot realize the global real-time synchronization of spectrum information. Grissa *et al.* [7] present a trustworthy framework for SAS. In each cluster, secondary users maintain a local blockchain and validators maintain a global blockchain. Members within clusters hold a light copy of the global blockchain containing the latest status of the system. Wang *et al.* [49] propose a layered multi-chain spectrum blockchain architecture for satellites and base stations, which is similar to [7], where regional blockchains are responsible for regional spectrum trading and regularly synchronize transaction information to the global blockchain. Wang *et al.* [37] design a two-phase confirmation mechanism to complete the communication and synchronization between two sub-chains in a satellite-terrestrial communication scenario. However, these efforts are not optimal for SANs because they depend on a multi-chain structure and require additional operations for cross-chain transactions, demanding significant resources from participants.

In order to reduce the overhead of blockchain in DSS, many efforts have focused on developing innovative consensus mechanisms. Zhu *et al.* [6] integrate the computation of the deep reinforcement learning-based method for solving the winner determination problem with the proof-of-work consensus mechanism. Fernando *et al.* [50] propose a proof-of-sense consensus mechanism, where the spectrum first sensor to successfully recovers a secret key transmitted randomly in a frequency band is rewarded. Ye *et al.* [51] introduce a proof-of-trust consensus mechanism that links participants' trust values with mining difficulty to reduce overhead in DSS. Notwithstanding the progress, these efforts still face challenges in terms of constrained flexibility and weak compatibility, and thus failing to be effectively applied in the involving SANs.

### C. Theoretical Analysis of Blockchain

To analyze the performance of blockchain in wireless networks, theoretical models are required. Sun *et al.* [18] establish an analytical model for the blockchain-enabled wireless system. Xu *et al.* [52] investigate the security performance

of wireless blockchain networks in the presence of malicious jamming for RAFT consensus mechanism. Wang *et al.* [37] analyze the probability of forking events in the intra-shard-transactions by considering the fading channel. However, the existing studies is for terrestrial networks and can not be directly applied in SANs due to the differences between terrestrial networks and SANs in terms of channel model, spatial distribution, and coverage condition.

To face the aforementioned challenges, we construct a blockchain-based architecture with a two-tier and multi-region design, however, it requires maintaining only one blockchain. Then, a spectrum-consensus integrated mechanism is proposed to enhance DSS efficiency and enable regions to dynamically innovate spectrum sharing schemes. Moreover, a theoretical framework which considers the unsteady and complex features of SANs is built to analyze the stability of PSC-DSS.

## VII. CONCLUSION AND DISCUSSION

This work proposes a partitioned, self-governed, and customized dynamic spectrum sharing approach for spectrum sharing between satellite access networks and terrestrial access networks. First, a sharded and tiered architecture is established to allows various regions to manage spectrum autonomously while jointly maintaining a single blockchain ledger. Then, a spectrum-consensus integrated mechanism is designed to enable parallel DSS and dynamical spectrum sharing schemes innovations. Finally, a theoretical framework is derived to justify the stability performance of the proposed approach. Simulations and experiments are conducted to validate the advantageous performance of PSC-DSS in terms of low-overhead, high efficiency, and robust stability.

Moreover, blockchain-based security is drawing growing interest from standardization and regulatory bodies. The 3rd Generation Partnership Project [53] and the European Telecommunications Standards Institute [54] have initiated discussions on leveraging blockchain to support decentralized trust and security in communication networks. The International Organization for Standardization [55] and ITU Telecommunication Standardization Sector [56] have also released technical reports and recommendations on blockchain security. These ongoing efforts lay the foundation for applying blockchain to spectrum sharing in SANs, while detailed technical standards are still lacking and require further research and development. From a regulatory standpoint, adopting blockchain-based dynamic spectrum sharing in SANs faces both opportunities and challenges. Although the FCC has expressed its interest in employing blockchain for this purpose [12], current regulatory frameworks generally rely on centralized mechanisms. As such, there exists a gap between the decentralized nature of blockchain solutions and the existing top-down regulatory models. For practical deployment, further regulatory adaptation and pilot studies are needed to assess how blockchain-based spectrum management can be aligned with compliance, accountability, and interference protection policies.

## APPENDIX A

In PSC-DSS, the intra-region interaction tolerates no more than  $\lfloor \frac{N_r}{3} \rfloor$  (i.e.,  $N_r = N_s + N_g$ ) faulty nodes (including satellites and ground nodes) based on PBFT consensus protocol (denoted as EVENT A), and the inter-regin interaction requires no more than  $\lfloor \frac{M}{2} \rfloor$  faulty regulators to commit a block (denoted as EVENT B). EVENT A includes two case: the regulator is not faulty (EVENT A0) and faulty (EVENT A1). However, EVENT A and EVENT B are not independent, as a faulty regulator in intra-region interaction can affect the consensus process in inter-region interaction. Thus, we have

$$P_S = \sum_{i=0}^{\lfloor \frac{N_r}{3} \rfloor} \Pr(A0) \times \Pr(A=i|A0) \times \Pr(B|A=i, A0) \\ + \sum_{i=1}^{\lfloor \frac{N_r}{3} \rfloor} \Pr(A1) \times \Pr(A=i|A1) \Pr(B|A=i, A1), \quad (19)$$

Here,  $\Pr(A0) = 1 - P_f^G$  and  $\Pr(A1) = P_f^G$ ,  $\Pr(A=i|A1)$  and  $\Pr(A=i|A0)$  presents the probabilities that there are  $i$  faulty nodes in intra-region interaction under the conditions that the regulator is faulty and not faulty, respectively. These probabilities are given as

$$\Pr(A=i|A0) = \sum_{n=0}^{\min(i, N_g-1)} P_{n0}, \quad (20)$$

and

$$\Pr(A=i|A1) = \sum_{n=1}^{\min(i, N_g)} P_{n1}, \quad (21)$$

with

$$P_{n0} = C_{N_g-1}^n (P_f^G)^n (1 - P_f^G)^{N_g-1-n} \times \mathbf{1}_{\{i-n < N_s\}} \\ \times C_{N_s}^{i-n} (P_f^S)^{i-n} (1 - P_f^S)^{N_s-(i-n)}, \quad (22)$$

$$P_{n1} = C_{N_g-1}^{n-1} (P_f^G)^{n-1} (1 - P_f^G)^{N_g-n} \times \mathbf{1}_{\{i-n < N_s\}} \\ \times C_{N_s}^{i-n} (P_f^S)^{i-n} (1 - P_f^S)^{N_s-(i-n)}, \quad (23)$$

where  $\mathbf{1}_{\{\cdot\}}$  is the indicator function.

$\Pr(B|A=i, A0)$  and  $\Pr(B|A=i, A1)$  indicates the probabilities of EVENT B occurring under the conditions that there are already  $i$  faulty nodes in intra-region interaction, with a faulty regulator and without a faulty regulator, respectively. The expressions for these probabilities are given as

$$\Pr(B|A=i, A0) = \sum_{j=0}^{\lfloor \frac{M}{2} \rfloor} P_j, \quad (24)$$

and

$$\Pr(B|A=i, A1) = \sum_{j=0}^{\lfloor \frac{M}{2} \rfloor - 1} P_j, \quad (25)$$

with

$$P_j = C_{M-1}^j (P_f^G)^j (1 - P_f^G)^{M-1-j}. \quad (26)$$

Thus, the expression of  $P_S$  can be given as (4).

## APPENDIX B

The relationship among  $N$ ,  $N_s + N_g$  and  $M$  is  $N = M \times (N_s + N_g) + 1 + \delta K$ . Let  $M = \frac{N - \delta K - 1}{N_r}$ , where  $N_r = N_s + N_g$ . Then, (17) can be expressed as

$$C = 2N_r^2 - 2N_r + 4K \frac{N - \delta K - 1}{N_r} - 4K + 5. \quad (27)$$

The first-order derivative and the second-order derivation of  $C$  with respect to  $N_r$  is

$$\frac{\partial C}{\partial N_r} = 4N_r - 2 - \frac{4K(N - \delta K - 1)}{N_r^2}, \quad (28)$$

and

$$\frac{\partial^2 C}{\partial N_r^2} = 4 + \frac{8K(N - \delta K - 1)}{N_r^3}. \quad (29)$$

respectively. Due to  $N - \delta K - 1 > 0$ , The minimum value of  $C$  can be reached at that zero point of the first-order derivative. According to Cardano formula [57], the zero point of the first-order derivative is given as

$$N_r = \frac{1}{3} + K^{\frac{1}{3}}(N - \delta K - 1)^{\frac{1}{3}}. \quad (30)$$

Then, substituting (30) into (27), we have the optimal value of  $C$  as (18).

## REFERENCES

- [1] 3GPP, "Study on new radio (NR) to support non-terrestrial networks (v15.4.0)," Sept. 2020.
- [2] ——, "Solutions for NR to support non-terrestrial networks (NTN): Non-terrestrial networks (NTN) related RF and co-existence aspects (v17.2.0)," Apr. 2023.
- [3] FCC, "Single network future: Supplemental coverage from space," 2024, Accessed: Mar. 15, 2024. [Online]. Available: <https://docs.fcc.gov/public/attachments/DOC-400678A1.pdf>
- [4] Z. Li, W. Wang, Q. Wu, and X. Wang, "Multi-operator dynamic spectrum sharing for wireless communications: A consortium blockchain enabled framework," *IEEE Trans. Cogn. Commun. Netw.*, vol. 9, no. 1, pp. 3–15, Feb. 2023.
- [5] R. H. Tehrani, S. Vahid, D. Triantafyllopoulou, H. Lee, and K. Moessner, "Licensed spectrum sharing schemes for mobile operators: A survey and outlook," *IEEE Commun. Surveys Tuts.*, vol. 18, no. 4, pp. 2591–2623, Jun. 2016.
- [6] K. Zhu, L. Huang, J. Nie, Y. Zhang, Z. Xiong, H.-N. Dai, and J. Jin, "Privacy-aware double auction with time-dependent valuation for blockchain-based dynamic spectrum sharing in IoT systems," *IEEE Internet of Things Journal*, pp. 1–1, Apr. 2022.
- [7] M. Grissa, A. A. Yavuz, and B. Hamdaoui, "TrustSAS: A trustworthy spectrum access system for the 3.5 GHz CBRS band," in *IEEE INFOCOM Conf. Comput. Commun.*, Paris, France, Apr. 2019, pp. 1495–1503.
- [8] F. Li, H. Yao, J. Du, C. Jiang, Z. Han, and Y. Liu, "Auction design for edge computation offloading in sdn-based ultra dense networks," *IEEE Trans. Mob. Comput.*, vol. 21, no. 5, pp. 1580–1595, May 2022.
- [9] Y. Xiao, S. Shi, W. Lou, C. Wang, X. Li, N. Zhang, Y. T. Hou, and J. H. Reed, "BD-SAS: Enabling dynamic spectrum sharing in low-trust environment," *IEEE Trans. Cogn. Commun. Netw.*, vol. 9, no. 4, pp. 842–856, Aug. 2023.
- [10] D. C. Nguyen, P. N. Pathirana, M. Ding, and A. Seneviratne, "Blockchain for 5g and beyond networks: A state of the art survey," *J. Netw. Comput. Appl.*, vol. 166, p. 102693, Sept. 2020. [Online]. Available: <https://www.sciencedirect.com/science/article/pii/S1084804520301673>
- [11] Z. Wang, B. Cao, Y. Sun, C. Liu, Z. Wan, and M. Peng, "Protecting system information from false base station attacks: A blockchain-based approach," *IEEE Trans. Wireless Commun.*, pp. 1–1, Jun. 2024.
- [12] L. Mearian, "FCC eyes blockchain to track, monitor growing wireless spectrums," 2019, Accessed: Apr. 1, 2024. [Online]. Available: <https://www.computerworld.com/article/3393179/fcc-eyes-blockchain-to-track-monitor-growing-wireless-spectrums.html>
- [13] China Communications Standards Association, "Research on blockchain based solutions for wireless network architecture," 2023, Accessed: Apr. 8, 2024. [Online]. Available: <https://www.ccsa.org.cn/webadmin/#/td-standardproject/projectplan/public>
- [14] State radio regulation of China, "France is experimenting with blockchain for spectrum management for the first time," 2018, Accessed: Apr. 1, 2024. [Online]. Available: <https://www.srrc.org.cn/article21248.aspx>
- [15] ZTE, "China unicorn 5g blockchain technology white paper," 2020, Accessed: Apr. 1, 2024. [Online]. Available: <https://chat.openai.com/c/c581b0dd-f0b9-4b0b-b359-4b8fdc6f7236>
- [16] 5GZORRO, "5g long term evolution," 2021, Accessed: Apr. 1, 2024. [Online]. Available: [https://www.5gzorro.eu/wp-content/uploads/2021/08/5GZORRO\\_D2.1\\_v1.5.pdf](https://www.5gzorro.eu/wp-content/uploads/2021/08/5GZORRO_D2.1_v1.5.pdf)
- [17] Y. Xiao, S. Shi, W. Lou, C. Wang, X. Li, N. Zhang, Y. T. Hou, and J. H. Reed, "Decentralized spectrum access system: Vision, challenges, and a blockchain solution," *IEEE Wirel. Commun.*, vol. 29, no. 1, pp. 220–228, Feb. 2022.
- [18] Z. Song, J. An, G. Pan, S. Wang, H. Zhang, Y. Chen, and M.-S. Alouini, "Cooperative satellite-aerial-terrestrial systems: A stochastic geometry model," *IEEE Trans. Wireless Commun.*, vol. 22, no. 1, pp. 220–236, Jan. 2023.
- [19] Z. Zhai, L. Zeng, T. Ouyang, S. Yu, Q. Huang, and X. Chen, "SECO: Multi-satellite edge computing enabled wide-area and real-time earth observation missions," in *IEEE Conference on Computer Communications*, Vancouver, BC, Canada., Apr. 2024, pp. 2548–2557.
- [20] Q. Tang, Z. Fei, B. Li, and Z. Han, "Computation offloading in leo satellite networks with hybrid cloud and edge computing," *IEEE Internet of Things Journal*, vol. 8, no. 11, pp. 9164–9176, Jun. 2021.
- [21] X. Zhang, J. Liu, R. Zhang, Y. Huang, J. Tong, N. Xin, L. Liu, and Z. Xiong, "Energy-efficient computation peer offloading in satellite edge computing networks," *IEEE Transactions on Mobile Computing*, vol. 23, no. 4, pp. 3077–3091, Apr. 2024.
- [22] J. Zhou, Q. Yang, L. Zhao, H. Dai, and F. Xiao, "Mobility-aware computation offloading in satellite edge computing networks," *IEEE Transactions on Mobile Computing*, vol. 23, no. 10, pp. 9135–9149, Oct. 2024.
- [23] M. Castro and B. Liskov, "Practical byzantine fault tolerance," in *Proc. 3rd Symp. Operating Syst. Des. Implementation*, 1999, pp. 173–186.
- [24] W. Li, C. Feng, L. Zhang, H. Xu, B. Cao, and M. A. Imran, "A scalable multi-layer pbft consensus for blockchain," *Trans. Parallel Distrib. Syst.*, vol. 32, no. 5, pp. 1146–1160, 2021.
- [25] D. Ongaro and J. Ousterhout, "In search of an understandable consensus algorithm," in *USENIX Annu. Techn. Conf. (USENIX ATC 14)*. Philadelphia, PA: USENIX Association, jun. 2014, pp. 305–319. [Online]. Available: <https://www.usenix.org/conference/atc14/technical-sessions/presentation/ongaro>
- [26] D.-H. Jung, J.-G. Ryu, and J. Choi, "When satellites work as eavesdroppers," *IEEE Trans. Inf. Forensics Security*, vol. 17, pp. 2784–2799, 2022.
- [27] H. Jia, C. Jiang, L. Kuang, and J. Lu, "An analytic approach for modeling uplink performance of mega constellations," *IEEE Trans. Veh. Technol.*, vol. 72, no. 2, pp. 2258–2268, 2023.
- [28] J. Park, J. Choi, and N. Lee, "A tractable approach to coverage analysis in downlink satellite networks," *IEEE Trans. Wireless Commun.*, vol. 22, no. 2, pp. 793–807, Feb. 2023.
- [29] D.-H. Jung, J.-G. Ryu, W.-J. Byun, and J. Choi, "Performance analysis of satellite communication system under the shadowed-rician fading: A stochastic geometry approach," *IEEE Trans. Commun.*, vol. 70, no. 4, pp. 2707–2721, Apr. 2022.
- [30] A. Al-Hourani, "An analytic approach for modeling the coverage performance of dense satellite networks," *IEEE Wireless Commun. Lett.*, vol. 10, no. 4, pp. 897–901, Apr. 2021.
- [31] Z. Wang, M. Cao, H. Jiang, B. Cao, S. Wang, C. Sun, and M. Peng, "Blockchain-enabled dynamic spectrum sharing for satellite and terrestrial communication networks," 2024, arXiv:2408.02013.
- [32] F. Tang, C. Wen, L. Luo, M. Zhao, and N. Kato, "Blockchain-based trusted traffic offloading in space-air-ground integrated networks (SAGIN): A federated reinforcement learning approach," *IEEE J. Sel. Areas Commun.*, vol. 40, no. 12, pp. 3501–3516, Dec. 2022.
- [33] Celestrak, "NORAD GP element sets current data," 2024, Accessed: Jun. 8, 2024. [Online]. Available: <https://celestrak.org/NORAD/elements/>

- [34] C. Mingrui, "Decoupling intra- and inter-shard consensus for high scalability in permissioned blockchain," 2024, Accessed: Jun. 8, 2024. [Online]. Available: <https://github.com/orgs/DP-Chain/repositories>
- [35] Google, "Spectrum access system," Accessed: Jun. 8, 2024. [Online]. Available: <https://cloud.google.com/spectrum-access-system/docs/overview?hl=en>
- [36] R. Zhu, H. Liu, L. Liu, X. Liu, W. Hu, and B. Yuan, "A blockchain-based two-stage secure spectrum intelligent sensing and sharing auction mechanism," *IEEE Trans. Ind. Informat.*, vol. 18, no. 4, pp. 2773–2783, Apr. 2022.
- [37] B. Wang, J. Jiao, S. Wu, R. Lu, and Q. Zhang, "Age-critical and secure blockchain sharding scheme for satellite-based internet of things," *IEEE Trans. Wireless Commun.*, vol. 21, no. 11, pp. 9432–9446, Nov. 2022.
- [38] MediaTek, "Mediatek 6g technology white paper: Satellite and terrestrial network convergence," 2023, Accessed: Mar. 15, 2023. [Online]. Available: [https://d86o2zu8ugzlg.cloudfront.net/mediatek-craft/documents/MediaTek\\_WhitePaper-6G-Satellite\\_EN0523F.pdf](https://d86o2zu8ugzlg.cloudfront.net/mediatek-craft/documents/MediaTek_WhitePaper-6G-Satellite_EN0523F.pdf)
- [39] H.-W. Lee, C.-C. Chen, C.-I. S. Liao, A. Medles, D. Lin, I.-K. Fu, and H.-Y. Wei, "Interference mitigation for reverse spectrum sharing in B5G/6G satellite-terrestrial networks," *IEEE Transactions on Vehicular Technology*, vol. 73, no. 3, pp. 4247–4263, Mar. 2024.
- [40] H.-W. Lee, A. Medles, V. Jie, D. Lin, X. Zhu, I.-K. Fu, and H.-Y. Wei, "Reverse spectrum allocation for spectrum sharing between tn and ntn," in *2021 IEEE Conference on Standards for Communications and Networking (CSCN)*, Thessaloniki, Greece, Dec. 2021, pp. 1–6.
- [41] L. Kułacz, H. Kokkinen, and A. Kliks, "Dynamic spectrum access in terrestrial and non-terrestrial networks," in *Proceedings of the 29th Annual International Conference on Mobile Computing and Networking*, ser. ACM MobiCom'23. New York, NY, USA: Association for Computing Machinery, Oct. 2023. [Online]. Available: <https://doi.org/10.1145/3570361.3615726>
- [42] H. Kokkinen, A. Piemontese, A. Reis-Kivinen, L. Kułacz, N. Borios, and C. Amatetti, "Proof of concept for spectrum sharing between terrestrial and satellite networks," in *2023 Joint European Conference on Networks and Communications and 6G Summit (EuCNC/6G Summit)*, Jun. 2023, pp. 276–281.
- [43] ESA, "ASCENT strategic recommendations: Spectrum sharing between satellite and terrestrial systems," 2020, Accessed: Oct. 25, 2020. [Online]. Available: <chrome-extension://efaidnbmnnibpcajpcgclefindmkaj/https://connectivity.esa.int/sites/default/files/ASCENT%20strategic%20recommendations%20-%20Whitepaper.pdf>
- [44] M. Jiang, Y. Li, Q. Zhang, G. Zhang, and J. Qin, "Decentralized blockchain-based dynamic spectrum acquisition for wireless downlink communications," *IEEE Trans. Signal Process.*, vol. 69, pp. 986–997, Jan. 2021.
- [45] G. O. Boateng, G. Sun, D. A. Mensah, D. M. Doe, R. Ou, and G. Liu, "Consortium blockchain-based spectrum trading for network slicing in 5G RAN: A multi-agent deep reinforcement learning approach," *IEEE Trans. Mobile Comput.*, vol. 22, no. 10, pp. 5801–5815, Oct. 2023.
- [46] D. Ayepah-Mensah, G. Sun, G. O. Boateng, S. Anokye, and G. Liu, "Blockchain-enabled federated learning-based resource allocation and trading for network slicing in 5G," *IEEE/ACM Trans. Netw.*, vol. 32, no. 1, pp. 654–669, Feb. 2024.
- [47] R. Xu, Z. Chang, X. Zhang, and T. Hämäläinen, "Blockchain-based resource trading in multi-uav edge computing system," *IEEE Internet Things J.*, pp. 1–1, Mar. 2024.
- [48] S. Hu, Y.-C. Liang, Z. Xiong, and D. Niyato, "Blockchain and artificial intelligence for dynamic resource sharing in 6g and beyond," *IEEE Wirel. Commun.*, vol. 28, no. 4, pp. 145–151, Aug. 2021.
- [49] W. Wang and Y. Zhao, "Blockchain-based spectrum management architecture and trading mechanism design for space-air-ground integrated network," *IEEE Communications Letters*, vol. 27, no. 10, pp. 2692–2696, Oct. 2023.
- [50] P. Fernando, K. Dadallage, T. Gamage, C. Seneviratne, A. Madanayake, and M. Liyanage, "Proof of sense: A novel consensus mechanism for spectrum misuse detection," *IEEE Trans. Ind. Informat.*, vol. 18, no. 12, pp. 9206–9216, Dec. 2022.
- [51] J. Ye, X. Kang, Y.-C. Liang, and S. Sun, "A trust-centric privacy-preserving blockchain for dynamic spectrum management in iot networks," *IEEE Internet Things J.*, vol. 9, no. 15, pp. 13 263–13 278, Aug. 2022.
- [52] H. Xu, L. Zhang, Y. Liu, and B. Cao, "RAFT based wireless blockchain networks in the presence of malicious jamming," *IEEE Wireless Commun. Lett.*, vol. 9, no. 6, pp. 817–821, Jun. 2020.
- [53] 3GPP, "Motivation for study on distributed device and user-centric trust," Accessed: Oct. 19, 2023. [Online]. Available: [https://www.3gpp.org/ftp/tsg\\_sa/WG1\\_Serv/TSGS1\\_104\\_Chicago/Docs](https://www.3gpp.org/ftp/tsg_sa/WG1_Serv/TSGS1_104_Chicago/Docs)
- [54] ETSI, "PDL for trustworthy 6G," Accessed: Oct. 19, 2023. [Online]. Available: [chrome-extension://efaidnbmnnibpcajpcgclefindmkaj/https://docbox.etsi.org/Workshop/2023/10\\_ETSISECURITYCONFERENCE/D42\\_6G/INTERDIGITAL\\_WANG.pdf](chrome-extension://efaidnbmnnibpcajpcgclefindmkaj/https://docbox.etsi.org/Workshop/2023/10_ETSISECURITYCONFERENCE/D42_6G/INTERDIGITAL_WANG.pdf)
- [55] ISO, "ISO/TR 23576:2020 Blockchain and distributed ledger technologies—Security management of digital asset custodians," Accessed: Jul. 6, 2024. [Online]. Available: <https://www.iso.org/standard/76072.html>
- [56] ITU-T, "X.1412: Security requirements for smart contract management based on the distributed ledger technology," Accessed: Jul. 6, 2023. [Online]. Available: <https://www.itu.int/rec/T-REC-X.1412-202304-I>
- [57] "Cardano formula," Accessed: Oct. 25, 2024. [Online]. Available: [https://encyclopediaofmath.org/wiki/Cardano\\_formula](https://encyclopediaofmath.org/wiki/Cardano_formula)



**Zixin Wang** received the M.E degree in information and communication engineering from Chongqing University of Posts and Telecommunications, Chongqing, China, in 2020. She currently is pursuing her Ph.D. degree in the State Key Laboratory of Networking and Switching Technology, Beijing University of Posts and Telecommunications, Beijing, China. Her research interests include blockchain and satellite networks.



**Mingrui Cao** received an undergraduate degree from the School of Computer Science and Engineering, University of Electronic Science and Technology of China, Chengdu, China, in 2021. He is currently pursuing the Ph.D. degree with the School of Information and Communication Engineering, Beijing University of Posts and Telecommunications, Beijing, China. His research interests include blockchain technologies, distributed systems and federated learning.



**Hao Jiang** received the B.E. degree in communication engineering from Chongqing University of Posts and Telecommunications, Chongqing, China, in 2022, and received the M.E. degree in information and communication engineering with the State Key Laboratory of Networking and Switching Technology, Beijing University of Posts and Telecommunications, Beijing, China, in 2025. His research interests include blockchain, resource allocation and satellite networks.

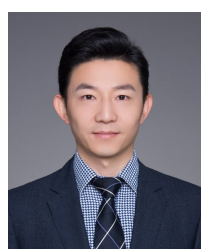


**Bin Cao** (Senior Member, IEEE) is a full professor in the State Key Laboratory of Network and Switching Technology at Beijing University of Posts and Telecommunications (BUPT). He received his Ph.D. degree with honors in Communication and Information Systems from the National Key Laboratory of Science and Technology on Communications at the University of Electronic Science and Technology of China (UESTC) in 2014. He was a research fellow at the National University of Singapore from July 2015 to July 2016. He has served and continues to

serve as an Associate Editor for IEEE Transactions on Mobile Computing and Digital Communications and Networks. He has been a Lead Guest Editor for journals such as the IEEE Internet of Things Journal, IEEE Communications Magazine, IEEE Network, and IEEE Wireless Communications. Additionally, he has co-chaired workshops for IEEE Global Blockchain 2024, the big data track of IEEE Globecom 2022, and the blockchain and web3.0 track of IEEE MetaCom 2023, among others. He has also been a TPC member for numerous conferences. He is the Founding Vice Chair of the Special Interest Group on Wireless Blockchain Networks in the IEEE Cognitive Networks Technical Committee. His awards include the IEEE Outstanding Leadership Award in 2020, the Best Paper Award at IEEE BMSB 2021, and the IEEE Technology and Engineering Management Society (TEMS) Mid-Career Award in 2021. His research interests are in blockchain systems, the internet of things, and mobile edge computing. He has published extensively in prestigious journals, including IEEE/ACM Transactions on Networking, IEEE Transactions on Parallel and Distributed Systems, and seven of his publications are ESI Hot/Highly Cited Papers.



**Shuo Wang** (Member, IEEE) received the Ph.D. degree in information and communications engineering from Beijing University of Posts and Telecommunications in 2019. He received the B.E. degree in information engineering from the Nanjing University of Aeronautics and Astronautics in 2011, and the M.E. degree in communication and information systems from the China Academy of Space Technology in 2014, respectively. From 2019 to 2021, he was a researcher with China Mobile Research Institute, working on 5G and 6G network architecture and participating in 3GPP service and system aspects (SA) standardization as a delegate. He is currently with the Wireless Network Research Department of Sony R&D Center, Beijing, China. His research focuses on dynamic spectrum sharing, blockchain, wireless sensing and 5G/6G standardization.



**Chen Sun** (S'02-M'05-SM'11) received a Ph.D. degree in electrical engineering from Nanyang Technological University, Singapore, in 2005. From August 2004 to May 2008, he was a researcher at ATR Wave Engineering Laboratories, Japan, working on adaptive beamforming and direction-finding algorithms for parasitic array antennas as well as theoretical analyses of cooperative wireless networks. In June 2008, he joined the National Institute of Information and Communications Technology (NICT), Japan, as an expert researcher working on distributed sensing

and dynamic spectrum access in TV white space. Since then, he has contributed to the IEEE 1900.6 standard, IEEE 802.11af standard and Wi-Fi Alliance specifications for Wi-Fi networks in TV white space. He served as the technical editor of the IEEE1900.6 standards and as a contributor to the IEEE 802.11af standards. He received the IEEE Standards Association IEEE 1900.6 Working Group Chair Award for leadership in 2011 and the IEEE 802.11af Outstanding Contributions Award in 2014. In 2021, he joined Sony China as a research manager working on the development of the IEEE 802.19, ETSI and 3GPP standards. He served as the 802.19 standard rapporteur for ETSI standards. He received the IEEE 802.19.1 Outstanding Contributions Award in 2018. He is currently the deputy head of Beijing Lab at Sony R&D Center. He is the author of the Handbook on Advancements in Smart Antenna Technologies for Wireless Networks, 40 international journal articles and more than 110 conference papers. He is also the first inventor of 80 granted patents in the US, EU, Japan, and China, including 9 patents that are worth more than 4 million dollars. His research interests include AI for beamforming, wireless federated learning, blockchain-based spectrum sharing, wireless sensing and V2X.



industrial internet.

**Liu Xing** (M'14) received the Ph.D. degree in Signal and Information Processing from Beijing University of Posts and Telecommunications, Beijing, China. He is the chief researcher, and the director of the industrial internet security research office in China Unicom Research Institute. He also served as an enterprise supervisor for doctoral students at Hunan University and an industry supervisor for postgraduates at Beijing University of Posts and Telecommunications. His research focuses on communication networks, mobile computing, and the security of



**Mugen Peng** (Fellow, IEEE) received the Ph.D. degree in communication and information systems from the Beijing University of Posts and Telecommunications (BUPT), Beijing, China, in 2005. In 2014, he was an Academic Visiting Fellow with Princeton University, Princeton, NJ, USA. He leads a Research Group focusing on wireless transmission and networking technologies with the State Key Laboratory of Networking and Switching Technology, BUPT. Dr. Peng was a recipient of the 2018 Heinrich Hertz Prize Paper Award, the 2014 IEEE ComSoc AP Outstanding Young Researcher Award. He is on the Editorial/Associate Editorial Board of the IEEE Communications Magazine and the IEEE Internet of Things Journal.